MARYLAND
ENVIRONMENTAL
SERVICE

Parris N. Glendening
Governor

James W. Peck
Director

October 1, 2002

Mr. Stephen Storms
Maryland Port Administration
Harbor Development
The Maritime Center II
2310 Broening Highway
Baltimore, Maryland 21224

RE: MPA Contract No. 500912, PIN No. 600105P
Environmental, Planning and Technical Services Agreement, Task 23

SUB: Submittal of the Poplar Island Modifications Option 6 Reconnaissance Study – Hydrodynamics and Sedimentation Modeling Draft Report

Dear Dr. Storms:

Please find enclosed 3 copies of the report entitled: *Poplar Island Modifications Option 6 Reconnaissance Study – Hydrodynamics and Sedimentation Modeling, Draft Report* prepared by Moffatt & Nichol Engineers (M&N).

Please review and comment on this report by Wednesday, October 16, 2002. Should you have any questions or comments on this submittal, please call me at 410 974-7261.

Sincerely,

Karen Cushman

Karen Cushman
Project Manager
Environmental Dredging

Enclosure

2011 Commerce Park Drive • Annapolis, Maryland 21401 • 410/974/7281 • Fax 410/974/7267

POPLAR ISLAND MODIFICATIONS
OPTION 6
RECONNAISSANCE STUDY

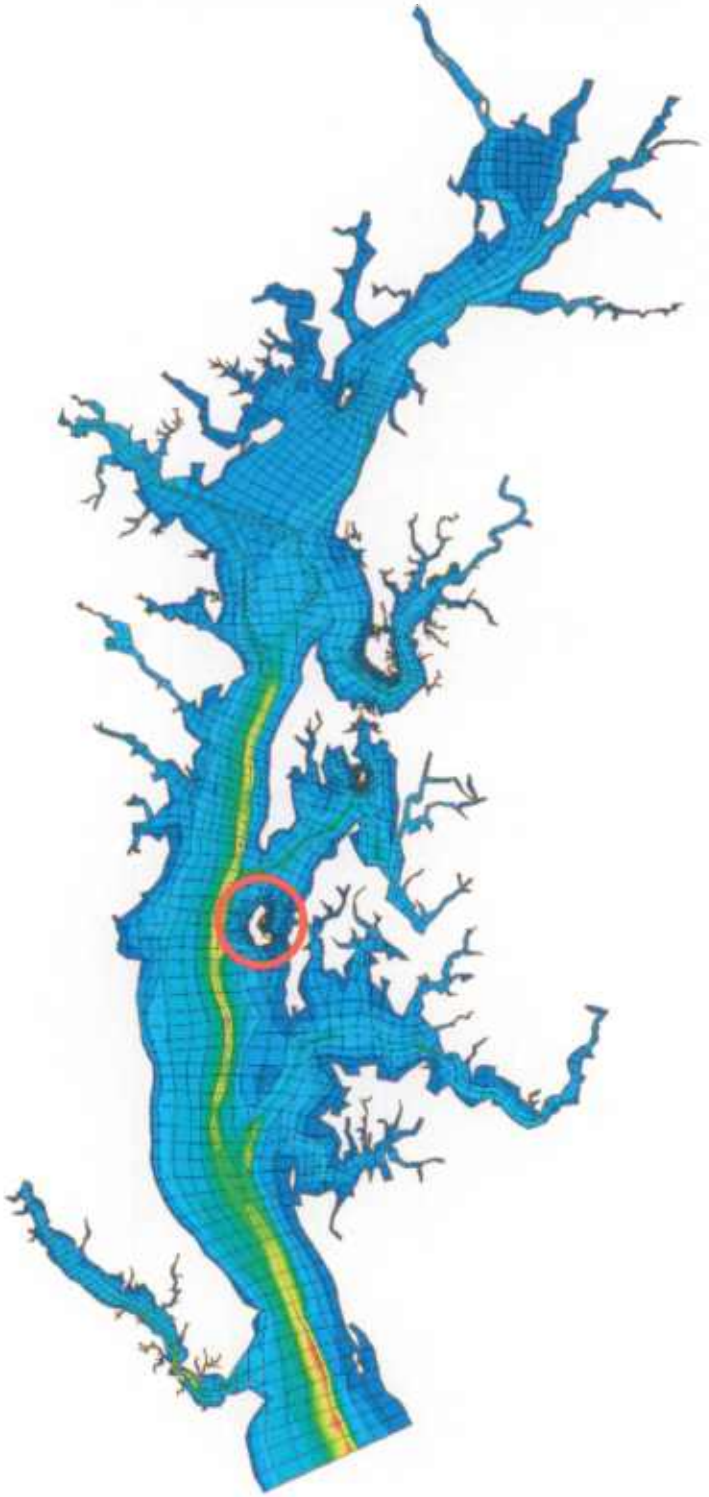

HYDRODYNAMICS AND SEDIMENTATION MODELING

DRAFT REPORT
SEPTEMBER 18, 2002

Maryland Port Administration
MPA Contract Number: 500912
MPA Pin Number: 600105-P

Maryland Environmental Services
MES Contract Number: 02-07-49

Prepared by

Moffatt & Nichol Engineers
2700 Lighthouse Point East
Suite 501
Baltimore, MD 21224

EXECUTIVE SUMMARY

The purpose of this Hydrodynamics and Sedimentation Modeling Reconnaissance Study is to evaluate the impacts of Modifications to the Poplar Island Environmental Restoration Project (PIERP). Moffatt & Nichol Engineers' (MNE) Upper Chesapeake Bay – Finite Element Model (UCB-FEM) (MNE, 2000) was used to predict existing conditions and with-project hydrodynamics and sedimentation. This report summarizes the calibration and implementation of the UCB-FEM two-dimensional numerical model of the Chesapeake Bay and evaluation of hydrodynamic and sedimentation output including time-varying flow velocity, water surface elevations, and patterns of erosion and accretion.

A summary of site conditions that are relevant to the project is provided below:

- **Bathymetry and Topography.** Water depths within the proposed modifications area vary from -1 ft and -10 ft MLLW; water depths in which the new containment dikes would be constructed range from -6 ft to -10 ft MLLW. Water depths in the deeper portions of the Bay west of the PIERP are approximately -124 ft MLLW.

- **Freshwater Inflow.** The drainage area of the Chesapeake Bay is approximately 64,000 square miles and includes portions of Maryland, Virginia, West Virginia, Pennsylvania, New York and the District of Columbia. Freshwater enters the Chesapeake Bay via approximately 150 major rivers and streams at approximately 80,000 cubic feet per second (Schubel, 1987).

- **Tides.** Water levels in the Chesapeake Bay are dominated by a semidiurnal lunar tide. Tides enter the Bay via the Chesapeake Bay entrance and the Chesapeake and Delaware (C&D) Canal. The mean range of tides throughout the entire Chesapeake Bay is generally 1 to 3 ft (NOS, 1988). In the project vicinity, the mean tide level is 0.9 ft above MLLW; the mean tidal range is 1.2 ft and the spring tidal range is 1.8 ft (NOS 1997).

- **Currents.** In the project vicinity, east of the south end of Poplar Island, peak tidal current velocities are approximately 1.7 ft/sec for flood currents and 1.0 ft/sec for ebb

currents (NOS, 1996). Approximately 2.5 miles west of Poplar Island, peak flood currents are about 1.0 ft/sec, and peak ebb currents are about 0.8 ft/sec. Currents are not considered to be important for shore protection design at this project site.

- **Wind and Wave Conditions.** Design winds for the site were developed on the basis of data collected at Baltimore-Washington International (BWI) airport. These winds, which can exceed 90 miles per hour during a 100-year storm event, were used to develop design wave conditions. Poplar Island is exposed to wind-generated waves approaching from all directions. For Option 6, the proposed dikes are protected from waves coming from the south and southwest directions.

- **Site Soil Characteristics.** Results of the preliminary study indicate that the underlying soil varies from silty clays to silty sands. The silty sands and preconsolidated silty clays are suitable for supporting the dike. However, areas with soft silty clays at the mud line would need to be undercut and backfilled with sand.

The numerical modeling system used in this study consists of the US Army Corps of Engineers finite element hydrodynamics (RMA-2) and sedimentation (SED-2D) models – collectively known as TABS-2 (Thomas and McAnally, 1985). The numerical modeling system uses a bathymetric mesh of water depths, represented by nodes located in the horizontal plane that are interconnected to create elements.

Correlation of the hydrodynamic model calibration results to NOAA predicted data for tidal elevations and current velocities is generally better than 90%. Predicted percent error is typically less than 10% for tidal elevations and less than 15% for current velocity.

The non-cohesive sediment model was run using 0.1mm (.004 inch) sediment under no-wind conditions. Analysis of results shows negligible sand transport due to tidal currents. Modeled non-cohesive sediment transport for existing conditions is negligible for 4- and 13-mph winds for all directions. Sixteen-mph winds, when taken cumulatively with lower wind speeds, account for nearly 90% of the yearly wind occurrences and cause significant sediment transport for winds from the NNW, N and NNE directions with negligible sediment transport for winds from other directions.

The cohesive sediment model was run for a 6-month simulation period at which point the model achieved a dynamic equilibrium (average values and rates remain steady over time). The cohesive sediment model was then run for each of 16 wind directions for wind speeds of 4-, 13-, and 16-mph.

Hydrodynamics and sedimentation numerical modeling for the Poplar Island Modifications – Option 6 Reconnaissance Study show that expansion of the PIERP would have minimal impacts on local tidal elevations and current velocities. Tidal elevations are unchanged, and maximum increase or decrease in current velocity is about 0.2 ft/sec. Construction of Option 6, however, would have significant beneficial effects on sedimentation rates and patterns. Option 6 would provide shelter to Poplar Harbor from wind and waves coming from the NNW, N, NNE and NE directions, causing reduced erosion of Jefferson Island and the shallow area of the harbor. This reduction in erosion would likely cause reduced suspended sediment and improved water quality within Poplar Harbor.

TABLE OF CONTENTS

LIST OF TABLES

LIST OF FIGURES

1. INTRODUCTION

1.1 STUDY PURPOSE AND OBJECTIVES

The purpose of this Hydrodynamics and Sedimentation Numerical Modeling Reconnaissance Study report is to analyze the impacts of the Modifications to the Poplar Island Environmental Restoration Project (PIERP) as regards hydrodynamics and sedimentation in the site vicinity. Moffatt & Nichol Engineers' (MNE) Upper Chesapeake Bay – Finite Element Model (UCB-FEM) (MNE, 2000) was modified to include the PIERP and used to predict with- and without-project hydrodynamics and sedimentation.

Study objectives include the following:

- Comparison of with- and without-project tidal elevations
- Comparison of with- and without-project current velocities
- Comparison of with- and without-project relative sedimentation rates and patterns for non-cohesive and cohesive sediments

The proposed Option 6 alignment is compared to existing conditions, both graphically and numerically, to determine both specific and relative impacts.

1.2 PROJECT SCOPE

The Modifications to the PIERP consist of expanding the existing facility for additional beneficial-use of dredged material. Benefits of this project include:

- Protection of Jefferson Island shoreline from additional erosion
- Additional protection of Poplar Harbor to provide improved water quality in the harbor and subsequently promote the re-establishment of subaquatic vegetation
- Creation of additional desirable habitats for fish and wildlife

To accomplish these objectives, Option 6 consists of the construction of armored dikes, breakwaters, and a sand beach north and east of the existing PIERP. The dikes would serve to contain clean sediments dredged from the Baltimore Harbor approach channels located within the Chesapeake Bay, whereas the breakwater and beach would serve to protect Poplar Harbor and Jefferson Island, in addition to providing desirable habitat.

1.3 STUDY DESCRIPTION

This report summarizes the calibration and implementation of a two-dimensional numerical model of the Chesapeake Bay to evaluate the impacts of the Poplar Island Modifications – Option 6 on tidal elevations, current velocity conditions, and sedimentation patterns in the vicinity of PIERP.

The existing UCB-FEM model was modified to provide additional detail near PIERP and was re-calibrated to published data, including astronomical tidal information, tidal current velocity information, and streamflow discharge for existing conditions. The calibrated model was used to compare hydrodynamic and sedimentation conditions within the model domain for the proposed construction alignment.

The UCB-FEM model was developed based on the following U.S. Army Corps of Engineers (USACE) numerical models:

- RMA-2: A depth-averaged finite element model for the simulation of velocities and water elevations for river systems, estuaries and other shallow water bodies. The model can be applied in either a one- or two-dimensional mode.

- SED-2D: A two-dimensional flow model for sediment transport related to unsteady flows. The model is based on the solution of the depth-averaged convection-diffusion equations of sediment with bed sources terms. SED-2D is capable of modeling cohesive and non-cohesive sediment transport.

Assumptions critical to these numerical modeling efforts include:

- Calibration and application of the UCB-FEM hydrodynamic model was performed

based on available data for normal tide and freshwater discharge conditions for existing conditions.

- Hydrodynamic conditions are analyzed to ascertain potential changes arising from Poplar Island Modifications.

- Sedimentation modeling was performed to estimate the change in bay sedimentation and scouring patterns and relative rates due to the Poplar Island Modifications.

- All results are subject to limitations of existing data, modeling capabilities and existing information regarding environmental resources and historical records. Hence, results depicted herein may be subject to modification in any additional future study stages as additional information is made available.

UCB-FEM hydrodynamic output includes time-varying flow velocity and water surface elevation fields. The UCB-FEM model also evaluates and predicts areas where erosion and accretion are likely to occur.

2. PROJECT SITE PHYSICAL CONDITIONS

2.1 GENERAL

Poplar Island is located in the Chesapeake Bay south of Kent Island, southeast of Eastern Bay and about 2 miles west of the eastern shore of Maryland. Modifications to the PIERP are being studied to expand the site for additional beneficial use of dredged material. The PIERP is located at approximately 38° 46' N latitude and 76° 23' W longitude (Maryland State Plane Coordinates N 401,000 E 1,490,000) as shown in Figure 2-1. Figure 2-2 is an aerial photograph of PIERP dated November 6, 2001. Figure 2-3 shows the proposed alignment for Option 6, a 314 acre expansion of the PIERP that consists of 157 acres of upland and 157 acres of wetland.

Site conditions germane to project design include bathymetry and topography, water levels, currents, wind and wave conditions, and site soil characteristics. A discussion of each of these factors is presented in the following paragraphs.

2.2 BATHYMETRY AND TOPOGRAPHY

The Chesapeake Bay is the largest estuary in the United States, extending over 200 miles from its seaward end at Cape Charles and Cape Henry in Virginia to the mouth of the Susquehanna River at Havre de Grace, Maryland. The Chesapeake Bay (including tributaries) has a surface area of approximately 4,500 square miles. Water depths in the Bay, including all of its tidal tributaries, average approximately 21 feet with a few deep troughs reaching a maximum depth of 174 feet (Schubel, 1987).

Chesapeake Bay bathymetric data was obtained from the National Ocean Service (NOS) Digital Elevation Models (NOS, 2000) and Charts 12230, 12263, 12264, 12266, 12268, 12270, 12272, 12273, 12274, and 12278. Vertical and horizontal data in this report are referenced to mean lower low water (MLLW) based on the 1960 to 1978 tidal epoch, and the Maryland State Plane, North American Datum 1983, respectively.

The bathymetry surrounding the PIERP is shown in Figure 2-3. Water depths within the proposed modifications area vary from -1 ft and -10 ft MLLW; water depths in which the new

containment dikes would be constructed range from -6 ft to -10 ft MLLW. Water depths in the deeper portions of the Bay west of the PIERP are approximately –124 ft MLLW.

2.3 FRESHWATER INFLOW

The drainage area of the Chesapeake Bay is approximately 64,000 square miles and includes portions of Maryland, Virginia, West Virginia, Pennsylvania, New York and the District of Columbia. Freshwater enters the Chesapeake Bay via approximately one-hundred and fifty major rivers and streams at approximately 80,000 cubic feet per second (Schubel, 1987). The primary rivers within the Chesapeake Bay drainage basin are the Susquehanna, Chester, Severn, Choptank, Patuxent, Nanticoke, Potomac, Rappahannock, York, and James Rivers. The Susquehanna River provides approximately 48.2% of the total freshwater inflow into the bay. Additional rivers on the western shore of the Bay, which contribute significant flows are the Potomac, James, Rappahannock, York, and Patuxent, contributing 13.6%, 12.5%, 3.1% 3.0% and 1.2%, respectively. Two significant sources of freshwater flow on the eastern shore of Maryland and Virginia are the Choptank (1.2%) and Nanticoke (1.1%) Rivers (Schubel, 1987).

2.4 TIDES

Water levels in the Chesapeake Bay are dominated by a semidiurnal lunar tide. Tides enter the Bay via the Chesapeake Bay Entrance and the Chesapeake and Delaware (C&D) Canal. The Bay is sufficiently long to contain one complete wavelength of the semidiurnal tide (NOS, 1988). The combination of tides and freshwater inflow creates a spring tide approximately 30-40% larger than mean tide and a neap tide approximately 30-40% smaller than the mean tide (Schubel, 1987).

The mean range of tides throughout the entire Chesapeake Bay is generally 1 to 3 feet (NOS, 1988). Tides are amplified in some tributaries as the tide progresses from the mouth of the tributary to the limit of the tide.

Average and spring tidal ranges, as published by NOS for the Bay north of the Potomac River (NOS Chart Nos. 12263, 12266, 12268, 12270, 12272), are listed in Table 2-1.

Table 2-1: Chesapeake Bay Tidal Ranges

Location	Mean Tidal Range (ft)	Spring Tidal Range (ft)
Main Chesapeake Bay		
Cove Point	1.3	2.0
Bloody Point Bar Light	1.3	1.6
Pooles Island	1.2	1.8
Sevenfoot Knoll Light	0.9	1.3
Western Chesapeake Bay		
Fairhaven, Herring Bay	0.9	1.3
Thomas Point Shoal Light	0.9	1.4
Annapolis	0.9	1.4
Sandy Point	0.8	1.2
Baltimore (Ft. McHenry)	1.2	1.7
Pond Point	1.4	2.1
Choptank River		
Cambridge	1.7	2.4
Chesapeake Beach	1.0	1.5
Eastern Bay		
St. Michaels, Miles River	1.2	1.8
Kent Island Narrows	1.2	1.8
Chester River		
Love Point	1.2	1.7
Queenstown	1.3	2.0
Cliffs Wharf	1.5	2.2
Chestertown	1.8	2.7
Sassafras River		
Betterton	1.6	2.4
C & D Canal		
Chesapeake City	2.8	2.9
Susquehanna River		
Havre de Grace	1.8	2.6

Average tides range from 0.8 ft in various locations on the western shore to 2.8 ft in the C & D Canal. Spring tides (tides occurring at or near the time of new or full moon which rise highest and fall lowest from the mean sea level) range from 1.3 ft at Fairhaven on Herring Bay to 2.9 ft in the C & D Canal. At the PIERP, mean tide range is approximately 1.2 ft (NOS, 1996).

Additionally, tides in the Chesapeake Bay are influenced by Coriolis forces (momentum forces due to the rotation of the Earth). Browne and Fisher (NOS, 1988) found a significant west to east tide range differential due to Coriolis forces throughout the bay with peak differences of 1.0 foot in the region between Smith Point (1 foot range, western shore) and Tangier Sound (2 foot range, eastern shore).

2.5 CURRENTS

Currents in the Chesapeake Bay are tidally driven and range in values up to a maximum velocity of over 3 ft/sec near the Bay entrance (NOS, 1988). Peak current velocities in the Bay north of Kent Island approach 1.5 ft/sec and average 1.2 ft/sec. Phasing of current velocity is influenced by bottom friction. Browne and Fisher (NOS, 1988) determined that during a given tidal cycle the peak current velocity occurs first in the center of the bay over the deepest channels, whereas peak velocity occurs later closer to shore in shallower water.

In the project vicinity east of the south end of Poplar Island, peak tidal current velocities are approximately 1.7 ft/sec for flood currents and 1.0 ft/sec for ebb currents (NOS, 1996). Approximately 2.5 miles west of Poplar Island, peak flood currents are about 1.0 ft/sec, and peak ebb currents are about 0.8 ft/sec.

2.6 WIND AND WAVE CONDITIONS

The frictional force of air on water as wind blows generates waves. Higher winds, deeper water, and longer distances over which the wind travels result in larger waves. Wind and wave conditions representative of the Poplar Island vicinity are discussed in the following paragraphs.

2.6.1 Wind Conditions

Average annual wind speeds at Poplar Island are represented by the wind rose shown in Figure 2-4. The wind rose represents percent occurrence of wind speeds and directions at Baltimore-Washington International (BWI) Airport as reported by the National Oceanic and Atmospheric Administration (NOAA), National Climatic Data Center (NOS, 1982 and NCDC, 1994). Table 2-2 shows the data used to generate the wind rose.

On average, nearly 90% of the yearly wind occurrences are less than 16 mph and only 1-2% of wind occurrences are greater than 25 mph.

Table 2-2: Wind Speed (% Occurrence) By Direction for BWI Airport, 1951-1982

Direction	0-3 MPH	4-13 MPH	13-16 MPH	16-19 MPH	19-25 MPH	25-32 MPH	>32 MPH
N		3.6	0.6	0.3	0.1	0	0
NNE		2.1	0.4	0.2	0.1	0	0
NE		3.3	0.5	0.2	0.1	0	0
ENE		3.3	0.6	0.3	0.1	0	0
E		4.3	0.5	0.2	0	0	0
ESE		2.3	0.2	0.1	0	0	0
SE		3.1	0.4	0.2	0.1	0	0
SSE		3.2	0.5	0.2	0.1	0	0
S		5.2	0.6	0.3	0.1	0	0
SSW		3.5	0.7	0.3	0.2	0	0
SW		4.7	0.8	0.4	0.2	0	0
WSW		4.7	0.6	0.3	0.1	0	0
W		9.4	1.4	1.0	0.7	0.2	0
WNW		5.9	1.8	1.5	1.3	0.4	0
NW		4.4	1.6	1.2	0.7	0.2	0
NNW		3.0	0.8	0.5	0.2	0	0
ALL	10.2						

Annual extreme wind speed data from the NOAA, NCDC for BWI Airport for the period 1951 through 1982 (NOS, 1982 and NCDC, 1994) are presented in Table 2-3 as fastest mile winds. Fastest mile winds are defined as the highest recorded wind speeds that last long enough to travel one mile during a 24-hour recording period. For example, a fastest mile wind speed of 60 miles per hour would have a duration of 60 seconds, a fastest mile wind speed of 50 miles per hour would have a duration of 72 seconds, etc.

Table 2-3: Annual Extreme Wind Speed (mph) Per Direction for BWI Airport, 1951-1982

Year	North	Northeast	East	Southeast	South	Southwest	West	Northwest
1951	24	41	27	34	39	29	42	46
1952	66	25	47	66	41	66	46	43
1953	20	28	22	27	34	39	47	43
1954	31	27	22	60	28	39	57	44
1955	21	43	29	28	43	53	40	43
1956	29	34	25	24	28	34	56	40
1957	29	53	35	33	33	30	46	46
1958	30	52	25	33	37	43	40	43
1959	28	26	20	27	23	38	46	43
1960	26	38	28	27	25	35	40	53
1961	45	28	28	29	24	70	41	54
1962	56	41	28	17	25	36	42	61
1963	38	32	18	34	25	28	44	60
1964	34	31	23	24	47	23	48	61
1965	36	26	28	34	36	54	44	44
1966	32	25	29	24	47	43	50	48
1967	30	29	25	39	27	46	53	43
1968	45	30	36	26	19	45	48	50
1969	28	21	20	34	26	45	45	53
1970	28	28	18	21	39	34	48	60
1971	31	45	26	18	21	41	39	58
1972	28	25	35	26	20	41	41	41
1973	40	26	26	38	26	35	49	33
1974	32	23	46	29	33	33	45	41
1975	40	26	21	24	25	38	54	45
1976	31	18	20	28	32	28	45	54
1977	32	31	19	28	26	25	49	48
1978	39	28	36	28	19	52	33	45
1979	32	25	27	36	32	32	45	47
1980	33	27	18	32	20	32	45	50
1981	24	24	19	26	23	28	41	42
1982	31	20	23	23	29	34	40	48

Note: Data adjusted to 10 meter height.

2.6.2 Wave Conditions

Poplar Island is exposed to wind-generated waves approaching from all directions. For Option 6, the proposed dikes are protected from waves coming from the south and southwest directions. In

accordance with procedures recommended by the U.S. Army Corps of Engineers (USACE), Shore Protection Manual (SPM) (USACE, 1984), a radially averaged fetch distance was computed for the other six directions. The radially averaged fetch distances for the N, NE, E, SE, W and NW directions for the Option 6 concept are shown in Table 2-4 and Figure 2-5.

Table 2-4: Radial Fetch Distance and Mean Water Depth at Poplar Island – Option 6

Direction	Mean Distance (Miles)	Mean Water Depth (ft, MLLW)
North	7.6	39.0
Northeast	10.5	19.6
East	2.1	9.0
Southeast	8.4	1.8
South	NA	NA
Southwest	NA	NA
West	8.6	30.0
Northwest	10.1	28.3

Wave conditions were hindcast along each fetch direction for the design winds presented in Table 2-3 (adjusted appropriately for duration) and the mean water depths along the fetch directions as shown in Table 2-4. Specifically, waves were hindcast for six directional design wind speeds (i.e. the design wind speeds computed for each individual direction) using methods published in the SPM (1984). Wave hindcast results are presented in Figure 2-6 (Significant Wave Height, H_s) and Figure 2-7 (Peak Wave Period, T_p). These figures present a summary of H_s and T_p showing the directions from which the highest waves and longest periods approach the site.

2.7 SITE SOIL CHARACTERISTICS

An evaluation of the soil characteristics at the project site was performed by Engineering Consultation Construction Remediation, Inc. (E2CR, 2002). The evaluation included performing soil borings, preparing soil boring profiles, identifying soil strata thickness, location and characteristics, and conducting a preliminary slope stability analysis. Results of the preliminary

study indicate that the underlying soil varies from silty clays to silty sands. The silty sands and preconsolidated silty clays are suitable for supporting the dike. However, areas with soft silty clays at the mud line would need to be undercut and backfilled with sand.

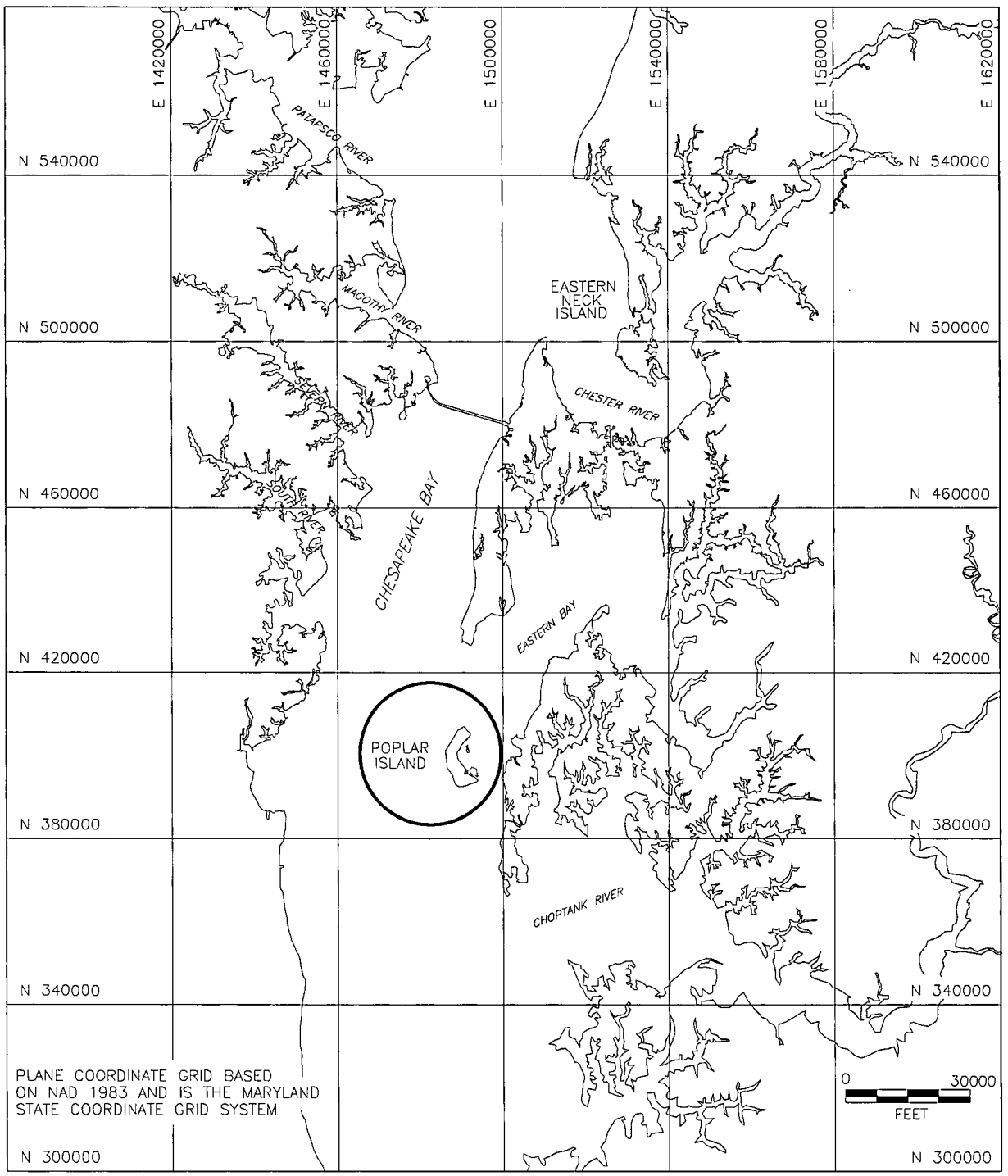

Figure 2-1: Poplar Island Location Map

Figure 2-2: Poplar Island Environmental Restoration Project November 2001 Aerial Photograph

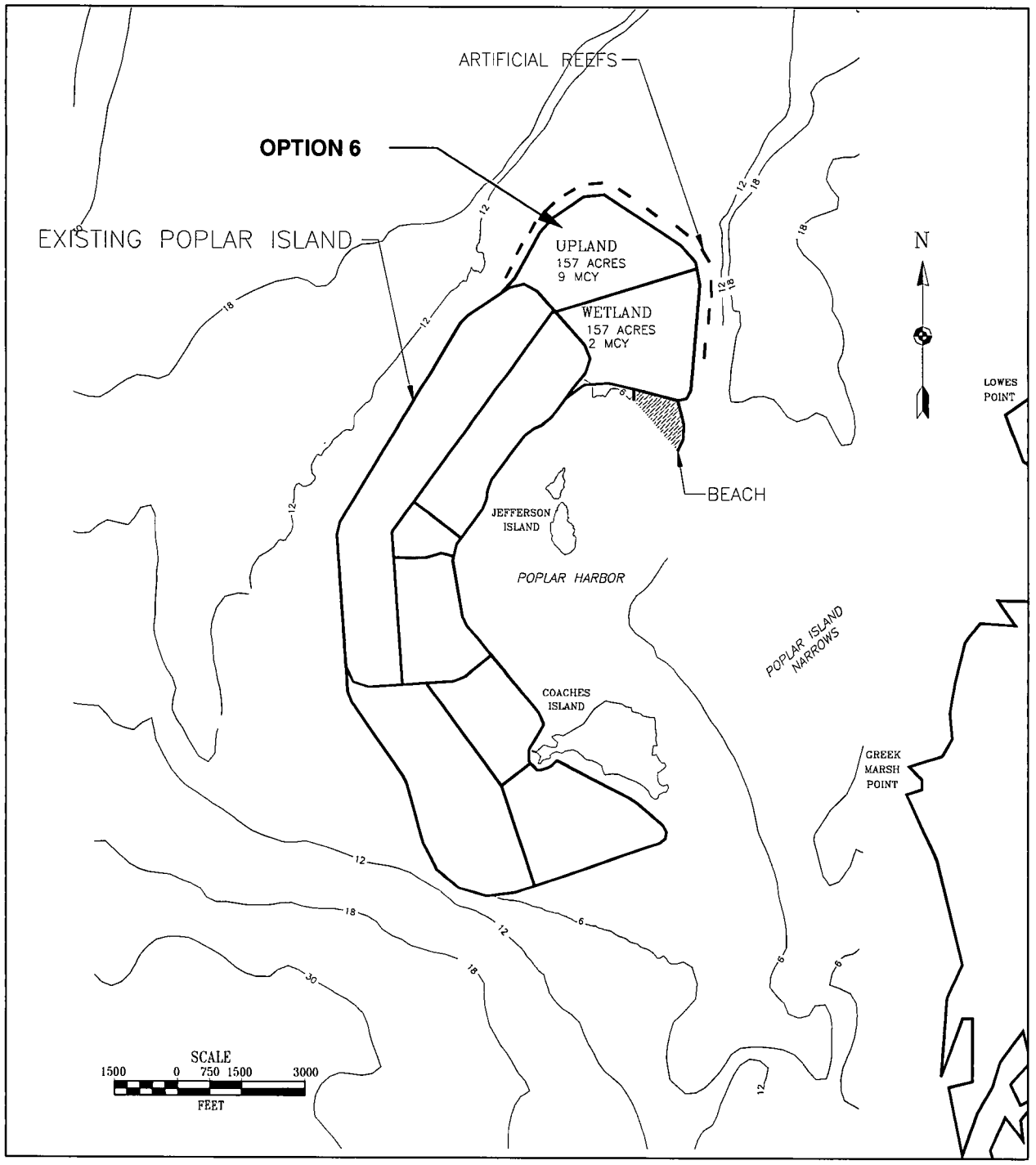

Figure 2-3: Poplar Island Option 6 and Site Bathymetry

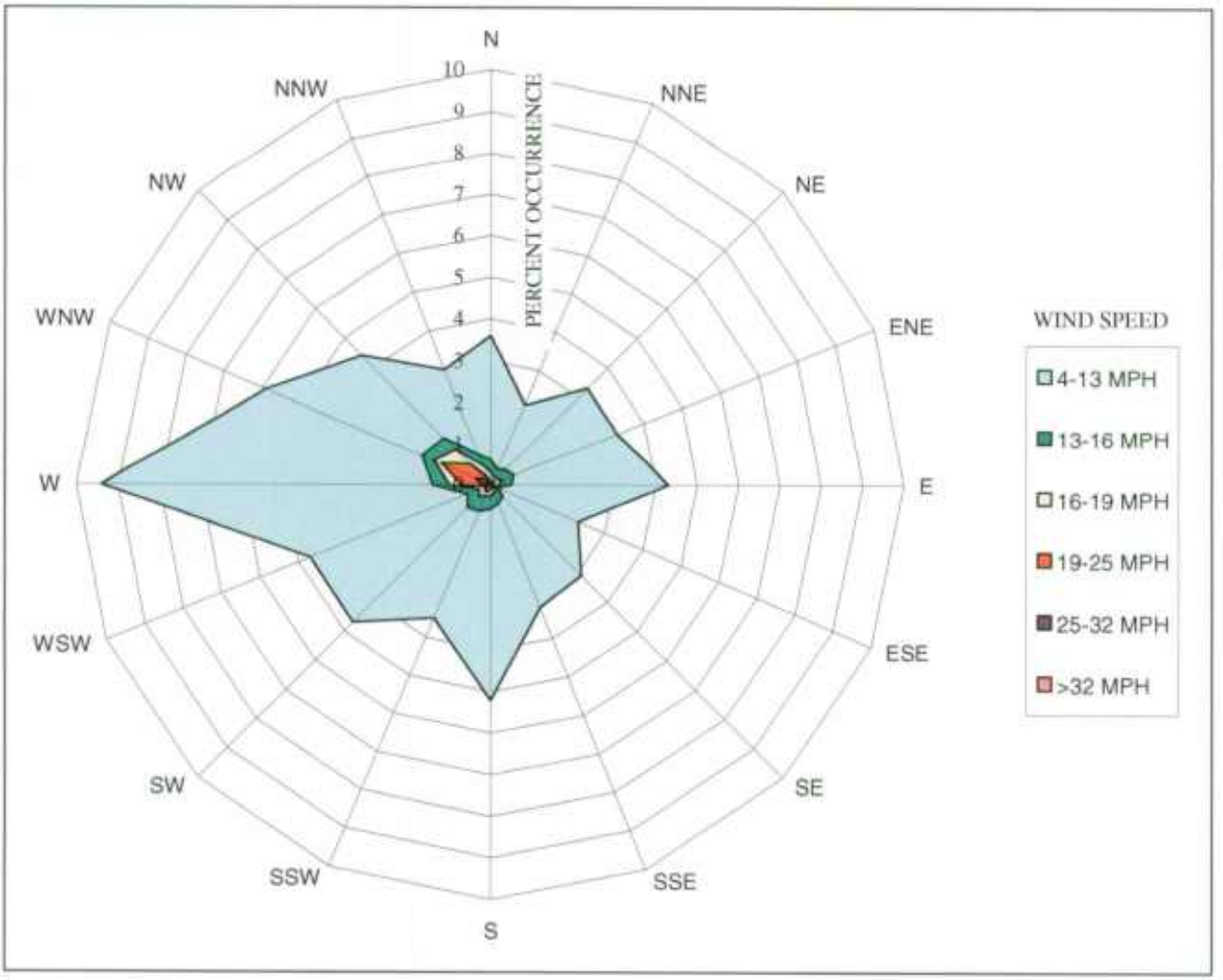

Figure 2-4: Baltimore-Washington International Airport (BWI) Wind Rose

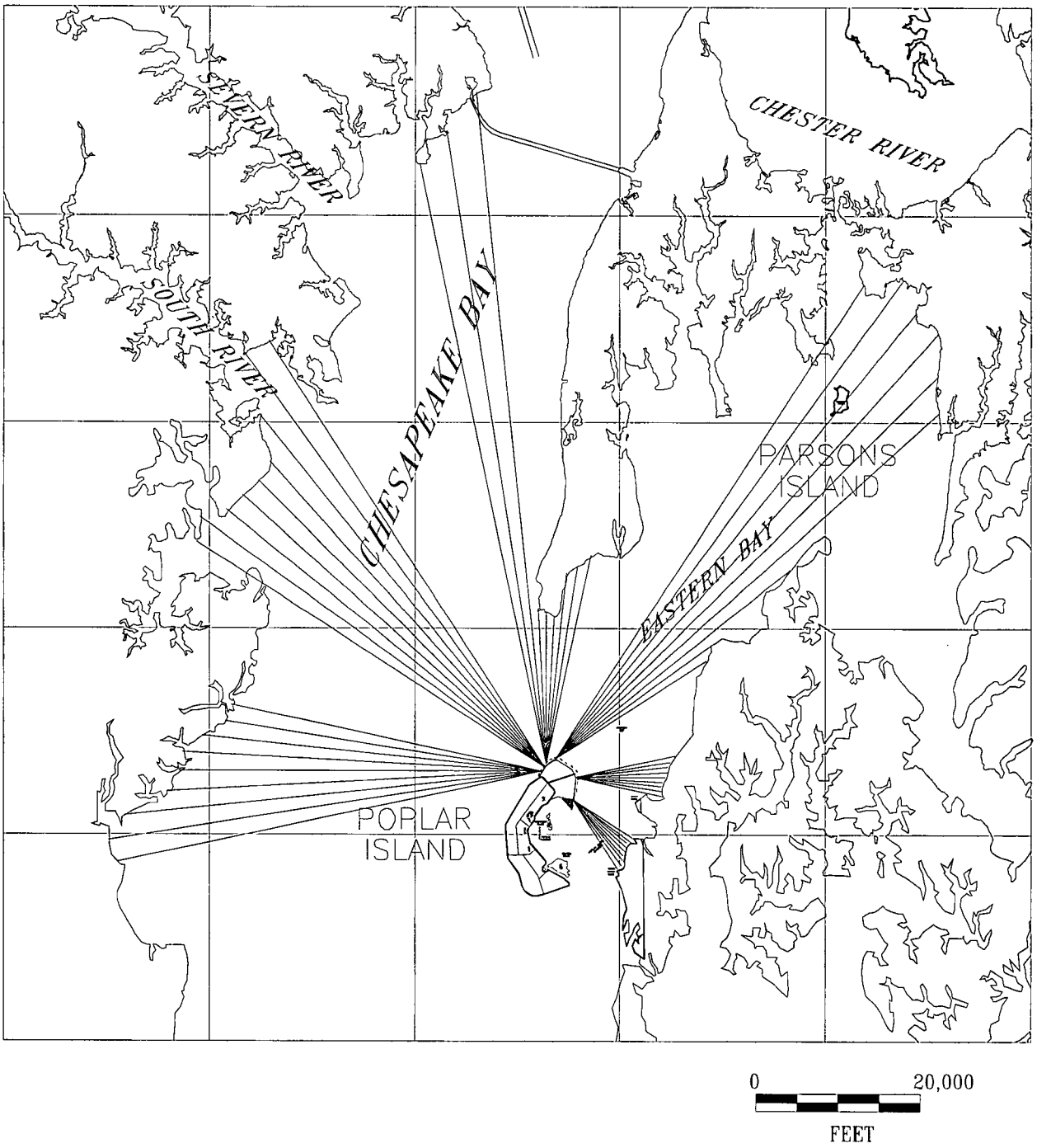

Figure 2-5: Poplar Island Option 6 Radially-Averaged Fetch Distances

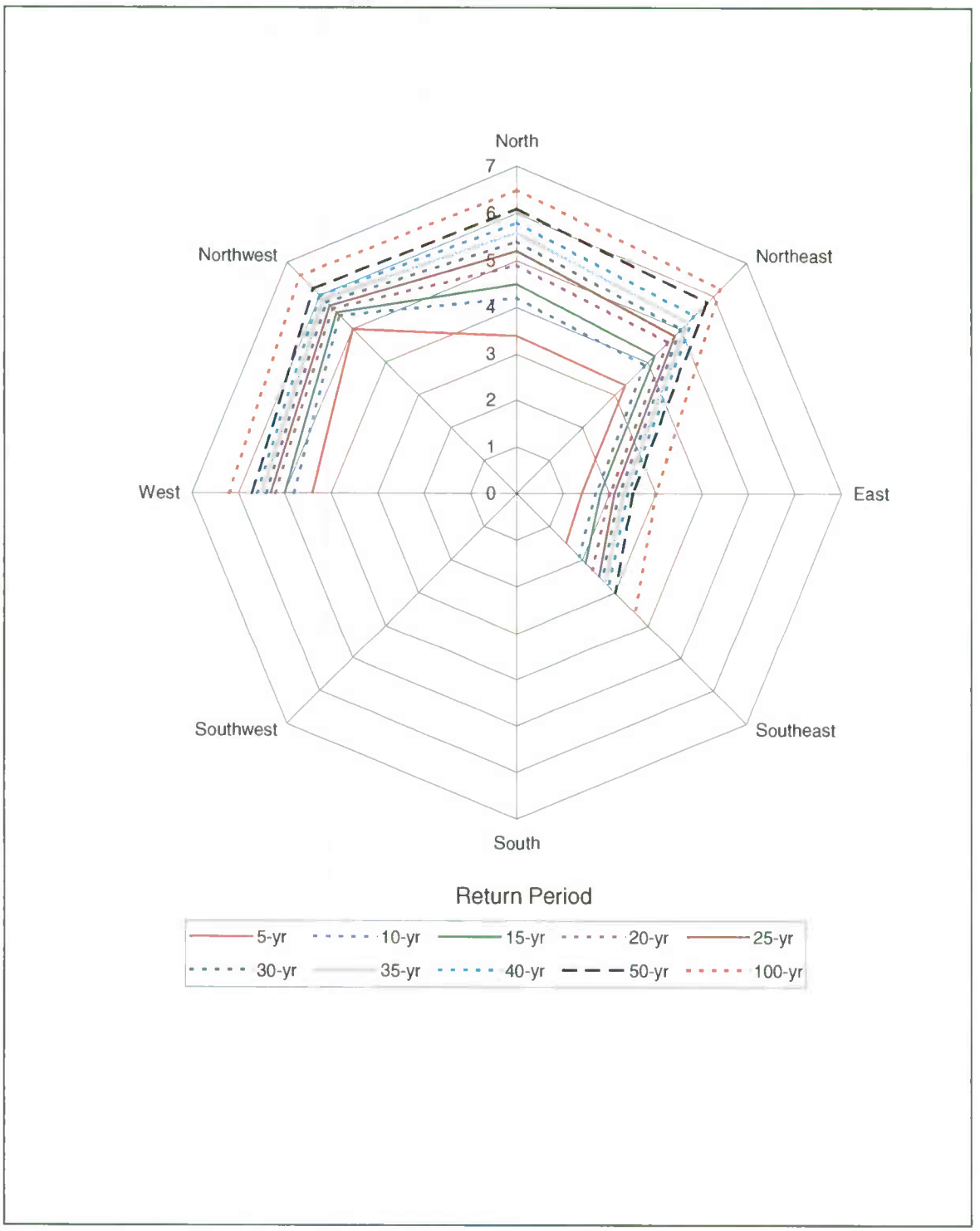

Figure 2-6: Nearshore Significant Wave Heights (ft) for Poplar Island – Option 6

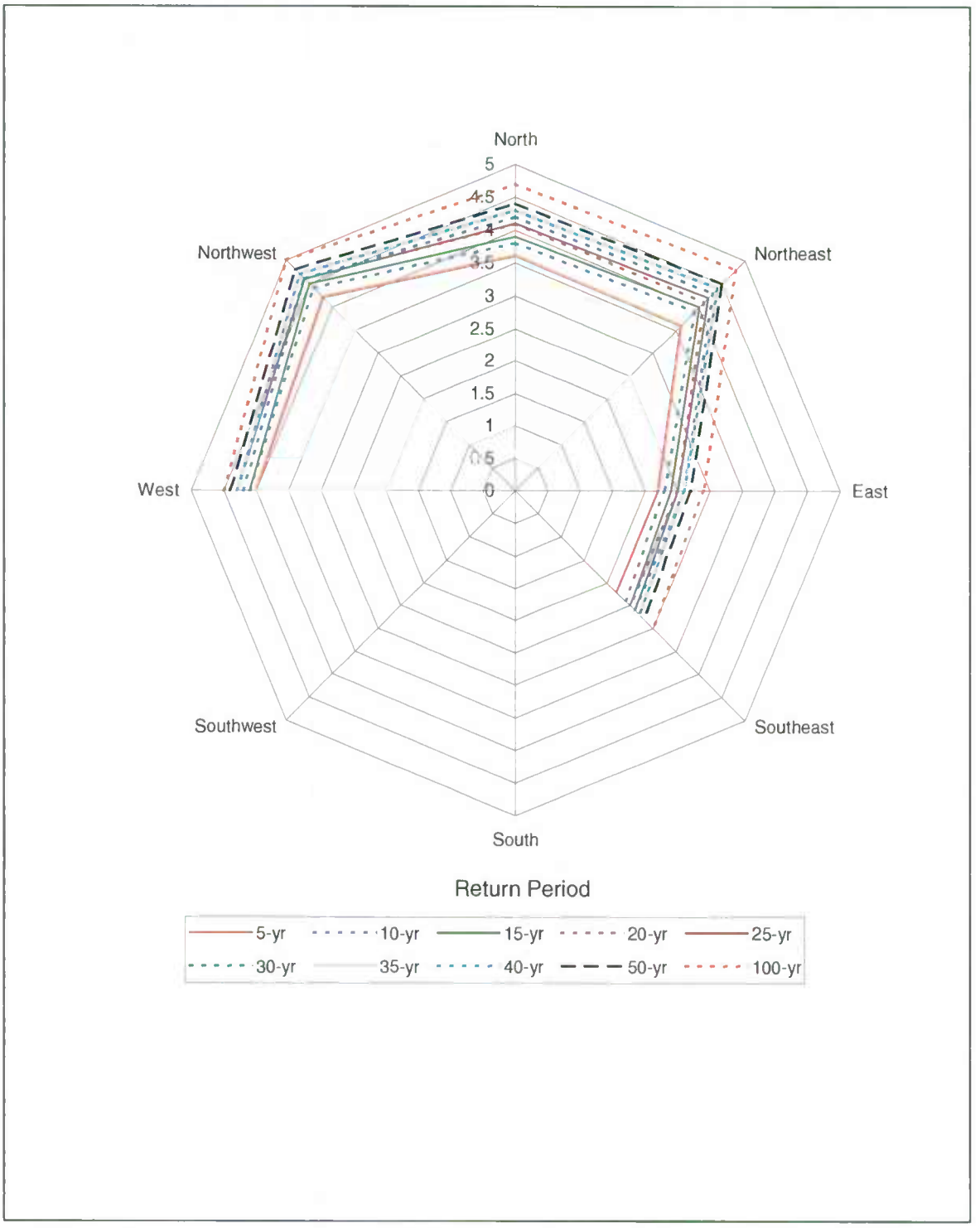

Figure 2-7: Peak Spectral Wave Periods (sec) for Poplar Island – Option 6

3. SIMULATION MODELS

3.1 GENERAL

The numerical modeling system used in this study is the US Army Corps of Engineers (USACE), Waterways Experiment Station (WES) finite element hydrodynamics (RMA-2) and sedimentation (SED-2D) models – collectively known as TABS-2 (Thomas and McAnally, 1985). TABS-2 is a collection of generalized computer programs and pre- and post-processor utility codes integrated into a numerical modeling system for studying two-dimensional depth-averaged hydrodynamics, constituent transport, and sedimentation problems in rivers, reservoirs, bays, and estuaries. The finite element method provides a means of obtaining an approximate solution to a system of governing equations by dividing the area of interest into smaller sub-areas called elements.

Time-varying partial differential equations are transformed into finite element form and then solved in a global matrix system for the modeled area of interest. The solution is smooth across each element and continuous over the computational area. This modeling system is capable of simulating wetting and drying of marsh and intertidal areas of the estuarine system.

A schematic representation of the system is shown in Figure 3-1. It can be used either as a stand-alone solution technique or as a step in the hybrid modeling approach. The model calculates water surface elevations, current patterns, constituent transport, sediment erosion and deposition, the resulting bed surface elevations, and the feedback to hydraulics. Existing conditions can be analyzed to determine the impacts of modifications to the PIERP on flow circulation and sedimentation. All models are depth-averaged and are solved by the finite element method using Galerkin weighted residuals.

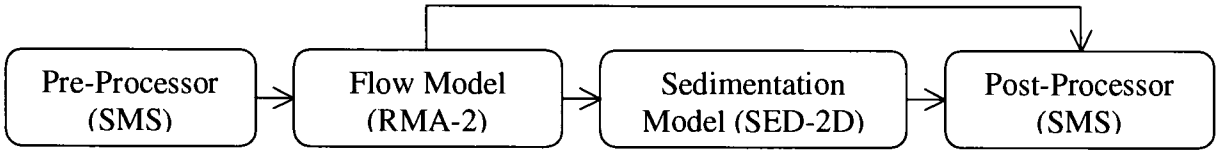

Figure 3-1: TABS-2 Schematic

3.2 HYDRODYNAMIC MODEL

RMA-2 is a two-dimensional, depth-averaged, finite element, hydrodynamic numerical model. It computes water surface elevations and horizontal velocity components for subcritical, free-surface flow in two dimensional flow fields. RMA-2 computes a finite element solution of the Reynolds form of the Navier-Stokes equations for turbulent flows. Friction is calculated with the Manning's or Chezy equation, and eddy viscosity coefficients are used to define turbulence characteristics. The equations also account for Coriolis forces and surface wind stresses. Both steady and unsteady state (dynamic) problems can be analyzed. The general governing equations are:

$$h\frac{\partial u}{\partial t}+hu\frac{\partial u}{\partial x}+hv\frac{\partial u}{\partial y}-\frac{h}{\rho}\left(E_{xx}\frac{\partial^2 u}{\partial x^2}+E_{xy}\frac{\partial^2 u}{\partial y^2}\right)+gh\left(\frac{\partial a}{\partial x}+\frac{\partial h}{\partial x}\right)+\frac{gun^2}{\left(1.486h^{1/6}\right)^2}+$$
$$(u^2+v^2)^{1/2}-\zeta V_a^2\cos\psi-2h\omega v\sin\phi=0$$

$$h\frac{\partial v}{\partial t}+hu\frac{\partial v}{\partial x}+hv\frac{\partial v}{\partial y}-\frac{h}{\rho}\left(E_{yx}\frac{\partial^2 v}{\partial x^2}+E_{yy}\frac{\partial^2 v}{\partial y^2}\right)+gh\left(\frac{\partial a}{\partial y}+\frac{\partial h}{\partial y}\right)+\frac{gvn^2}{\left(1.486h^{1/6}\right)^2}+$$
$$(u^2+v^2)^{1/2}-\zeta V_a^2\sin\psi-2h\omega v\sin\phi=0$$

$$\frac{\partial h}{\partial t}+h\left(\frac{\partial u}{\partial x}+\frac{\partial v}{\partial y}\right)+u\frac{\partial h}{\partial x}+v\frac{\partial h}{\partial y}=0$$

where:

- h = Depth
- u,v = Velocities in Cartesian directions
- x,y,t = Cartesian coordinates and time
- ρ = Density of fluid
- E = Eddy viscosity coefficient
  - for xx = normal direction on x-axis surface
  - for yy = normal direction on y-axis surface
  - for xy and yx = shear direction on each surface

g = Acceleration due to gravity

a = Elevation of Bottom

n = Manning's roughness n-value

1.486 = Conversion from SI (metric) to non-SI units

ζ = Empirical wind shear coefficient

V_a = Wind speed

Ψ = Wind direction

ω = Rate of Earth's angular rotation

ϕ = Local latitude

RMA-2 operates under the hydrostatic assumption, meaning accelerations in the vertical direction are negligible. RMA-2 is two dimensional in the horizontal plane and is not intended for use in near field problems where vortices, vibrations, or vertical accelerations are of primary interest. Vertically stratified flow effects are beyond the capabilities of RMA-2.

3.3 SEDIMENTATION MODEL

The sedimentation model, SED-2D, can be applied to sediments where flow velocities can be considered two-dimensional in the horizontal plane (i.e., the speed and direction can be satisfactorily represented as a depth-averaged velocity). It is useful for both deposition and erosion studies. The program treats two categories of sediment: 1) noncohesive, which is referred to as sand herein; and 2) cohesive, which is referred to as clay.

Both clay and sand may be analyzed, but the model considers a single, effective grain size during each simulation. Therefore, a separate model run is required for each effective grain size. Fall velocity must be prescribed along with the water surface elevations, x-velocity, y-velocity, diffusion coefficients bed density, critical shear stresses for erosion, erosion rate constants, and critical shear stress for deposition.

The derivation of the basic finite element formulation is presented in Ariathurai (1974) and Ariathurai, MacArthur, and Krone (1977) and is summarized below.

There are four major computations.

1. Convection-Diffusion Governing Equation
2. Bed Shear Stress Calculation
3. The Bed Source/Sink Term
4. The Bed Strata Discretization

3.3.1 Convection-Diffusion Governing Equation

The mesh employed for the hydrodynamic model is used for the sedimentation model. The convection-dispersion equation in two horizontal dimensions for a single sediment constitute solved by the model is:

$$\frac{\partial C}{\partial t} + u\frac{\partial C}{\partial x} + v\frac{\partial C}{\partial y} = D_x\frac{\partial^2 C}{\partial x^2} + D_y\frac{\partial^2}{\partial y^2} + \alpha_1^C + \alpha_2$$

where:

u,v = depth-averaged sediment velocity components
C = suspended sediment concentration
D_x = effective diffusion coefficient in X-direction
D_y = effective diffusion coefficient in Y-direction
□ = concentration-dependent source/sink term
□ = coefficient of source/sink term

The source/sink terms in the above equation are computed in routines that treat the interaction of the flow and the bed. Separate sections of the code handle computations for clay bed and sand bed problems as described below.

3.3.2 Bed Shear Stress

Bed shear stresses are calculated from the flow speed according to one of four optional equations: the smooth-wall log velocity profile or Manning equation for flows alone; and a smooth bed or rippled bed equation for combined currents and wind waves. Shear stresses are

calculated using the shear velocity concept where

$$\tau_b = \rho u_*^2$$

where:

□ = bed shear stress

u_* = shear velocity

and the shear velocity is calculated by one of four methods:

a. Smooth-wall log velocity profiles

$$\frac{\bar{u}}{u_*} = 5.75 \log\left(3.32 \frac{u_* h}{\nu}\right)$$

which is applicable to the lower 15 percent of the boundary layer when

□

where □ is the mean flow velocity (resultant of u and v components)

b. The Manning shear stress equation

□

where CME is a coefficient of 1 for SI (metric units) and 1.486 for non-SI units of measurement.

c. A Jonsson-type equation for surface shear stress (plane beds) caused by waves and currents

$$u_* = \sqrt{\frac{1}{2}\left(\frac{f_w u_{om} + f_c \bar{u}}{u_{om} + u}\right)\left(\bar{u} + \frac{u_{om}}{2}\right)}$$

where

f_w = shear stress coefficient for waves

u_{om} = maximum orbital velocity of waves

f_c = shear stress coefficient for currents

d. A Bijker-type equation for total shear stress caused by waves and current

$$u_* = \sqrt{\frac{1}{2} f_c \bar{u}^2 + \frac{1}{4} f_w u_{om}^2}$$

3.3.3 Source/Sink Terms

The Ackers-White (1973) procedure is used to calculate a sediment transport potential for sand from which actual sand transport is calculated based on sediment availability. Model clay erosion is based on formulas by Partheniades (1962) and Ariathurai while the deposition of clay utilizes Krone's equations (Ariathurai, MacArthur, and Krone, 1977).

3.3.3.1 Sand Transport

For sand transport, the transport potential of the flow and availability of material in the bed control the supply of sediment from the bed. The bed source term is

$$S = \frac{C_{eq} - C}{t_c}$$

where:

S = source term

C_{eq} = equilibrium concentration (transport potential)

C = sediment concentration in the water column

t_c = characteristic time for effecting the transition

There are many transport relations for calculating C_{eq} for sand size material. The Ackers-White (1973) formula was adopted for this model because it performed satisfactorily in tests by WES and others (White, Milli, and Crabbe 1975; Swart1976), is relatively complete, and is reasonably simple. The transport potential is related to sediment and flow parameters by the expressions in the following paragraphs. The Ackers-White formula computes the total load, including suspended load and bed load, and was developed originally for fine sand. The formulation was later updated to include coarser sands and these revised coefficients are included in the current model formulation. However, the appropriateness of the use of SED-2D with the Ackers-White formula diminishes with coarsening of the sediment.

The characteristic time, t_c, is somewhat subjective. It should be the amount of time required for the concentration in the flow field to change from C to C_{eq}. In the case of deposition, t_c is related to fall velocity. The following expression was adopted.

$$t_c = \text{the larger of} \begin{cases} C_d \dfrac{h}{V_s} \\ or \\ DT \end{cases}$$

where:

t_c = Characteristic time

C_d = Coefficient for deposition

V_s = Fall velocity of a sediment particle

DT = Computational time interval

In the case of scour, there are no simple parameters to employ. The following expression is used.

$$t_c = \text{the larger of} \begin{cases} C_e \frac{h}{u} \\ or \\ DT \end{cases}$$

where:

C_e = Coefficient for entrainment

V = Flow speed

3.3.3.2 Clay Transport

Cohesive sediments (usually clays and some silts) are considered to be depositional if the bed shear stress exerted by the flow is less than a critical value □. When that value occurs, the deposition rate is given by Krone's (1962) equation

$$S = \begin{cases} -\frac{2V_s}{h} C\left(1 - \frac{\tau}{\tau_d}\right) \text{ for } C < C_c \\ -\frac{2V_s}{hC_c^{4/3}} C^{5/3}\left(1 - \frac{\tau}{\tau_d}\right) \text{ for } C > C_c \end{cases}$$

where:

S = source term

V_s = fall velocity of a sediment particle

h = flow depth

C = sediment concentration in water column

τ = bed shear stress

□ = critical shear stress for deposition

C_c = critical concentration = 300 mg/□

If the bed shear stress is greater than the critical value for particle erosion □, material is removed from the bed. The source term is then computed by Ariathuarai's (Ariathurai, MacArthur, and

Krone 1977) adaptation of Partheniades' (1962) findings:

where P is the erosion rate constant, unless the shear stress is also greater than the critical value for mass erosion. When this value is exceeded, mass failure of a sediment layer occurs and

$$S = \frac{T_L \rho_L}{h \Delta t} \text{ for } \tau > \tau_s$$

where:

T_L = thickness of the failed layer

ρ_L = density of the failed layer

Δt = time interval over which failure occurs

$\square$ = bulk shear strength of the layer

3.3.4 Bed Strata Discretization

The sink-source term in convection-diffusion equation becomes a source-sink term for the bed model, which keeps track of the elevation, composition, and character of the bed.

3.3.4.1 Sand Beds

Sand beds are considered to consist of a sediment reservoir of finite thickness, below which is a nonerodible surface. Sediment is added to or removed from the bed at rate determined by the value of the sink/source term at the previous and present time-steps. The mass rate of exchange with the bed is converted to a volumetric rate of change by the bed porosity parameter.

3.3.4.2 Clay Beds

Clay beds are treated as a sequence of layers. Each layer has its own characteristics as follows:

- Thickness.
- Density.

- Age.
- Bulk shear strength.
- Type.

In addition, the layer type specifies a second list of characteristics.

- Critical shear stress for erosion.
- Erosion rate constant.
- Initial and 1-year densities.
- Initial and 1-year bulk shear strengths.
- Consolidation coefficient.
- Clay or sand.

New clay deposits form layers up to a specified initial thickness and then increase in density and strength with increasing overburden pressure and age. Variation with overburden occurs by increasing the layer type value by one for each additional layer deposited above it.

4. FINITE ELEMENT MESH

4.1 GENERAL

The numerical modeling system implemented herein requires that a database of water depths and bottom material properties represent the estuarial system. Water depths are represented by nodes located in the horizontal plane, which are interconnected to create elements. Two, three, or four nodes can be connected to form elements. The resulting nodal/element network is commonly called a finite element mesh and provides a computerized representation of the estuarial geometry and bathymetry.

4.2 ELEMENTS

RMA-2 is capable of supporting different types of elements within the same computational finite element mesh. The types of elements fit into three basic categories:

- Two Dimensional Elements
- One Dimensional Elements
- Special Elements

These element types are discussed briefly in the following sections.

4.2.1 Two Dimensional Elements

Two-dimensional elements are the customary type used with RMA-2 and may be either triangular or quadrilateral in shape, as shown in Figure 4-1. A two dimensional element possesses a length and a width, determined by the positions of the corner nodes which define the element. The depth at any location within a two dimensional element is obtained by interpolating among the depths of the corner nodes which define the element.

Quadrilateral Element **Triangular Element**

Figure 4-1: Finite Element Shapes

4.2.2 One Dimensional Elements

A one-dimensional element is a simplified element which is composed of two corner nodes and one midside node. The Finite Element Governing Equations for one-dimensional elements are based on a trapezoidal cross section with side slopes, and an off channel storage area. The depth at any location along a one-dimensional element is obtained by interpolating between the depths of the two corner nodes defining the element.

4.2.3 Special Elements

Special elements are one-dimensional elements that serve special purposes including transition from one- to two-dimensional elements, junctions between multiple one-dimensional elements, and flow control structures.

4.3 MODEL EXTENTS

The areal extent and the level of detail necessary to represent the project area are the parameters that define a finite element mesh. The TABS-2 system, described in Section 3.0, is numerically robust and capable of simulating tidal elevations, flows, and sediment transport over a mesh with widely varying boundaries and levels of detail. Accordingly, the incorporation of significant bathymetric features of the estuary generally dictates the level of detail for the mesh. However, there are several factors used to guide decisions regarding the extents of the mesh. First, it is desirable to extend the mesh to areas sufficiently distant from the project site such that the boundary conditions do not directly influence the hydrodynamics at the site. Secondly, the terminus of the mesh should be in a location where conditions can be reasonably measured and described to the model. Additionally, it is preferable to locate boundaries in locations where flow characteristics have been measured or are known and can be accurately specified.

Geometric information for the UCB-FEM model was obtained from NOAA DEMs, nautical charts, and recently performed bathymetric surveys. NOAA DEM's are electronic maps of bathymetric elevations imposed on a 30-meter grid and are based on many years of hydrographic survey data acquired for production of navigational charts. For the areas not covered by the DEM, navigation charts were used to complete the mesh. The resulting mesh geometry was checked and alterations were made as deemed necessary to improve physical representation of the estuary and to improve model stability in areas of large depth gradients.

The UCB-FEM model finite element mesh used herein is shown in Figure 4-2. Quadrilateral and triangular 2-dimensional elements were used to represent the estuarial system. The southern boundary of the mesh is located in the Chesapeake Bay near the Hooper Island Light from which it extends north to its terminus at the Conowingo Dam on the Susquehanna River and Chesapeake City on the C & D Canal resulting in total mesh length of roughly 90 nautical miles. A dense mesh was created around Poplar Island to provide a more accurate simulation of conditions at the project site.

Water depths were adjusted to represent both existing and with-project conditions. Figure 4-3 depicts the finite element mesh developed for existing conditions in the vicinity of Poplar Island. Figure 4-4 depicts the finite element mesh developed for Option 6.

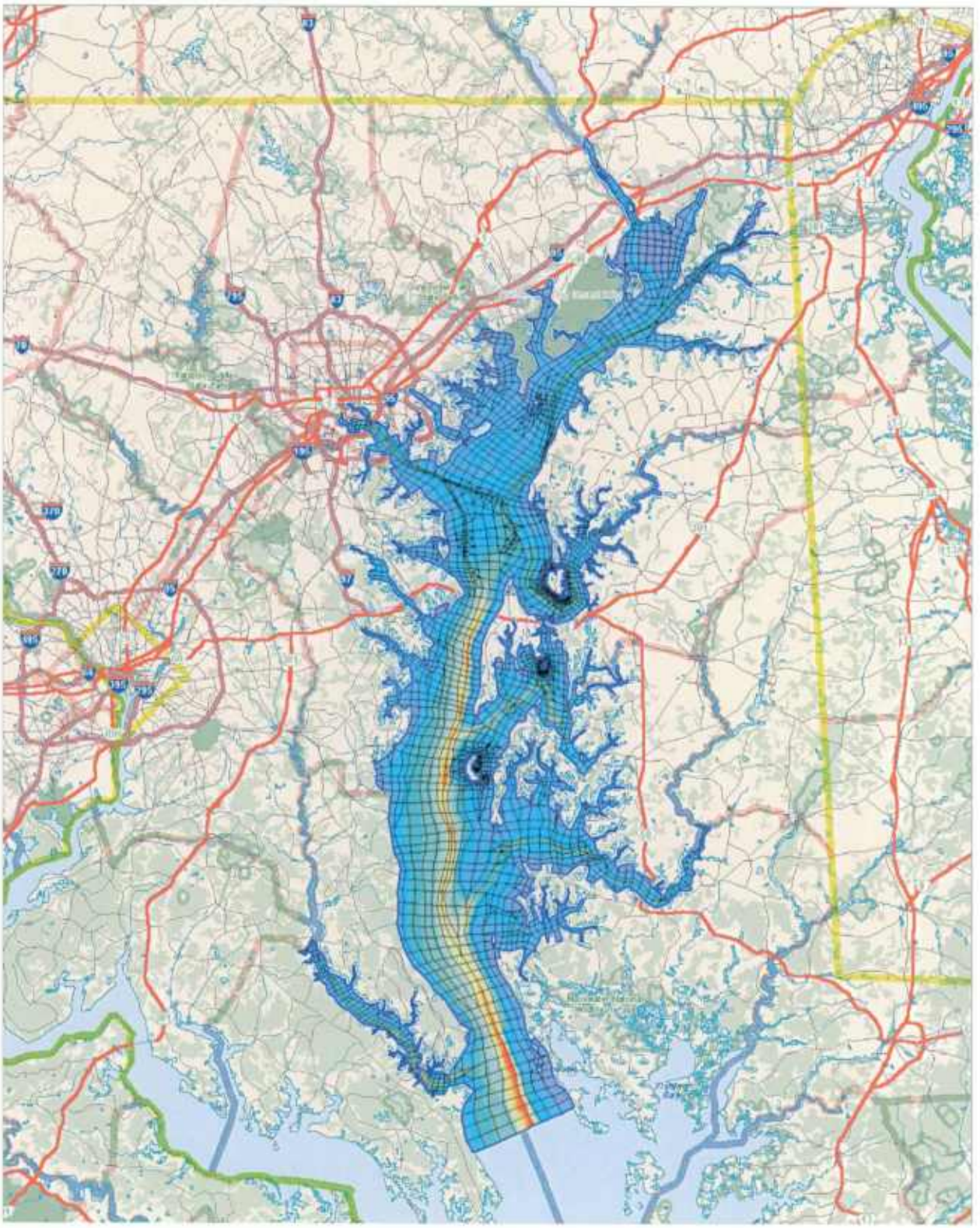

Figure 4-2: Upper Chesapeake Bay Finite Element Model (UCB-FEM)

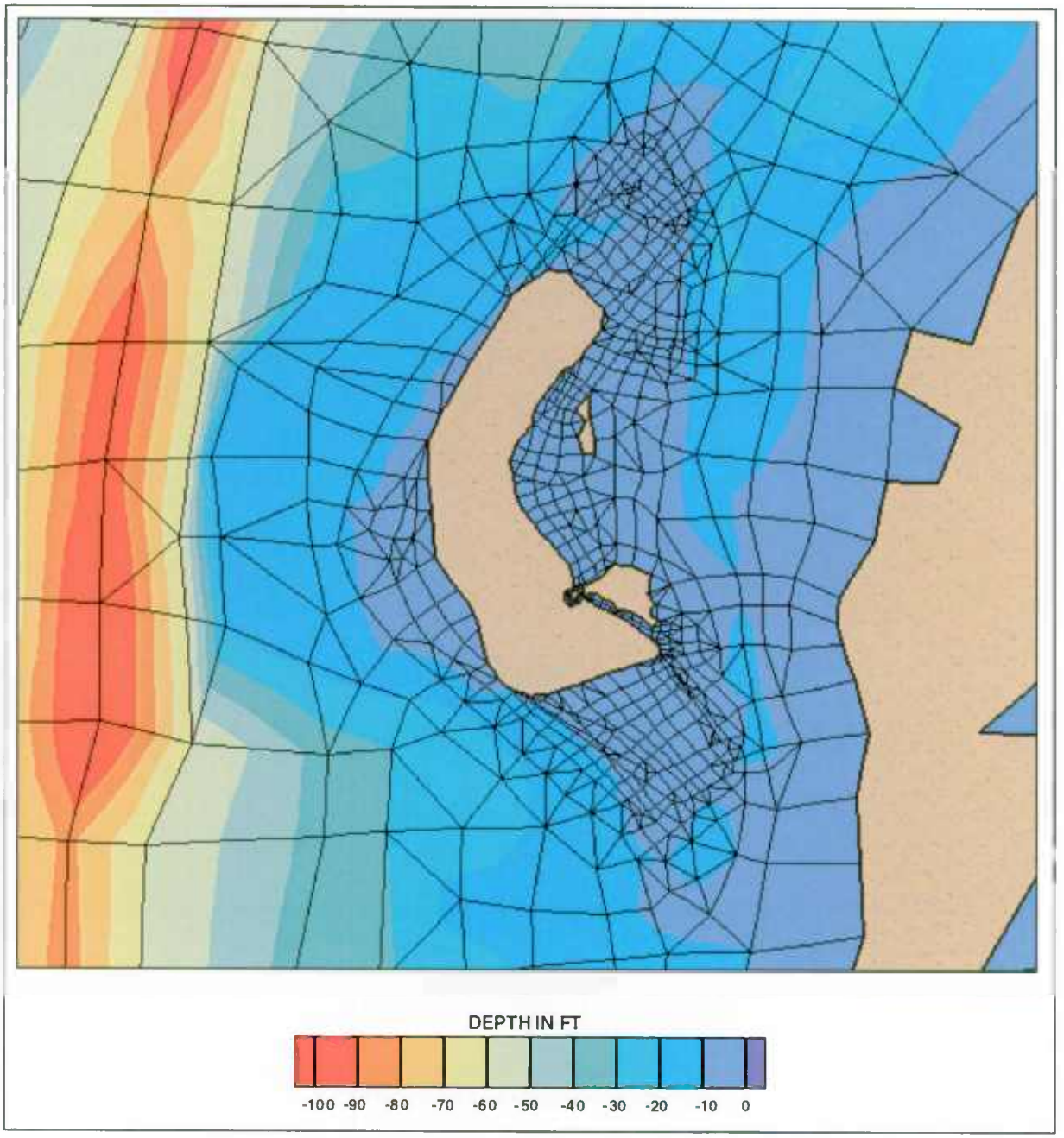

Figure 4-3: UCB-FEM – PIERP Existing Conditions

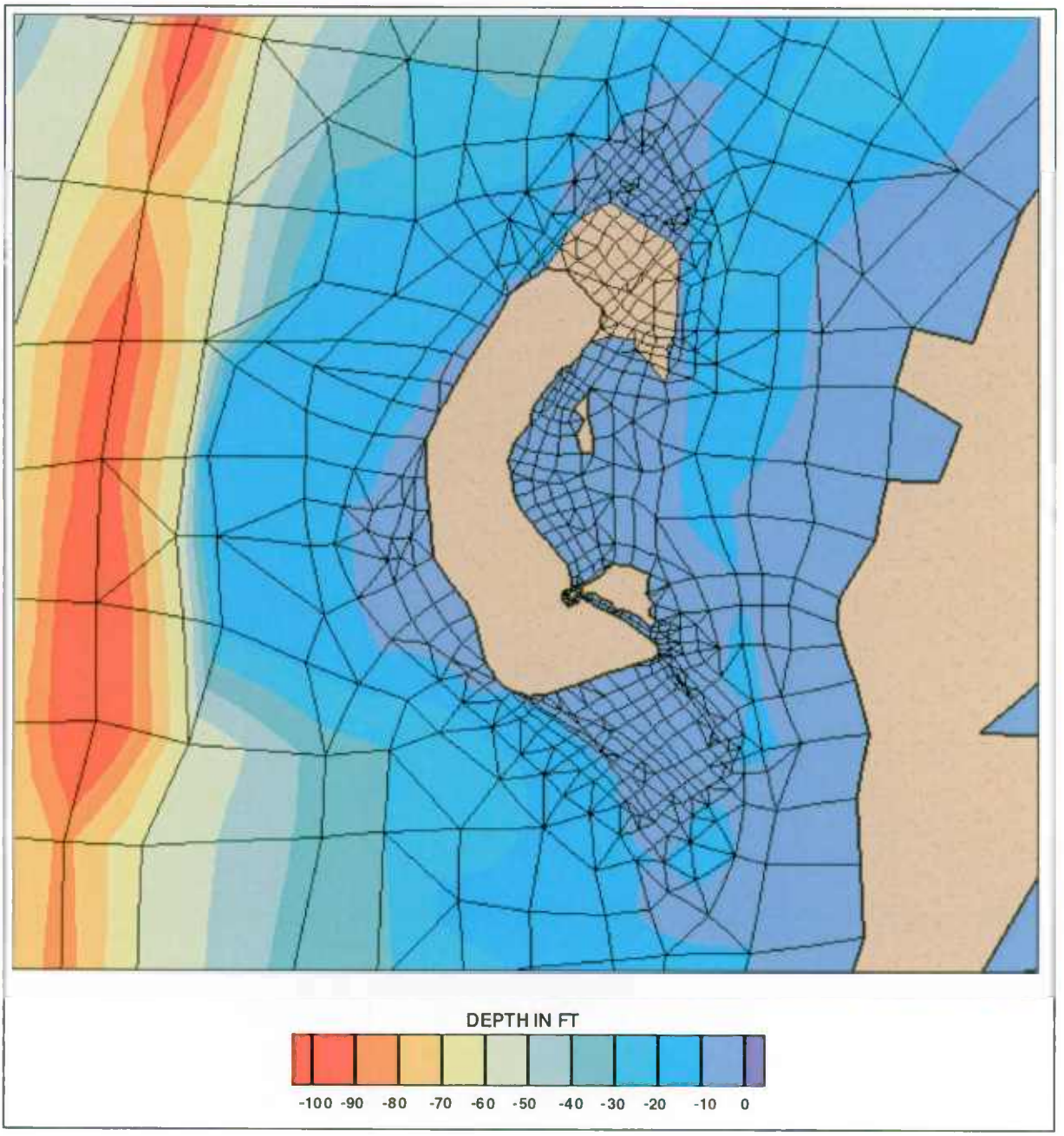

Figure 4-4: UCB-FEM – PIERP with Option 6

5. MODEL CALIBRATION

5.1 GENERAL

A measure of a finite element model's accuracy is the comparison of modeled tide elevations and currents with measured or known values. A properly calibrated model can be expected to produce current velocity and tidal elevation results with 80% to 100% accuracy. Model calibrations are adjusted by the refinement of the model bathymetry, the accurate representation of bottom structure (i.e. vegetation, mud, sand) and the stipulation of model parameters that are artifacts of the numerical formulation and are functions of element size and empirical constants. Upon satisfactory completion of calibration, the model can be used to evaluate the impacts of physical changes to the system.

Model calibration is best achieved by means of a set of simultaneous measurements both along the model boundaries and throughout the estuarial system. Boundary conditions important to the present study include tidal elevation, flow velocity, freshwater discharge, suspended sediment concentration, and bottom change over time. For a given set of boundary conditions, the model should be calibrated to reproduce tidal elevations, tidal velocities, or sedimentation rates and patterns within the estuary. The sediment transport model is driven by results obtained from the hydrodynamic model; therefore, the latter is calibrated first.

5.2 HYDRODYNAMIC MODEL

The UCB-FEM model is controlled by boundary conditions as shown in Figure 5-1. Boundary conditions are located on the southern boundary of the model in the vicinity of the Hooper Island Light and at the Conowingo Dam on the Susquehanna River and Chesapeake City on the C & D Canal on the northern boundaries. Additional boundary conditions are stipulated at tributaries throughout the model domain including the Patuxent, Choptank, Chester, and Susquehanna Rivers as well as the other smaller tributaries listed in Table 5-1. The type of boundary condition is based on the data available at each boundary. The Hooper Island Light boundary condition is comprised of tidal elevations while the C & D Canal, Patuxent River, Chester River and Choptank River boundary conditions consist of current velocities and directions and the

Conowingo Dam boundary condition is described by volume flux (flow). Boundary conditions located at smaller tributaries are described as constant sources of flow into the bay based on historic average measured flow. Calibration was performed for a two-week period of predicted data from February 1-14, 2001, which is representative of an average tidal cycle and low freshwater inflow.

Table 5-1: Freshwater Inflow Boundaries

Location	Flowrate (cfs)
Patapsco River	431
Gunpowder River	2888
Bush River	1149
Elk River	1874

Tide elevation and current velocity boundary conditions for the UCB-FEM model are based on NOS tidal predictions. NOS tidal predictions are based on historic harmonic constituents and represent idealized conditions which do not account for low frequency events including wind and storms. Figure 5-2 shows the water surface elevations and current velocities used as boundary conditions in the UCB-FEM model calibration.

Aside from the boundary conditions, the model is also influenced by bottom friction and eddy viscosity. Physically, bottom friction varies by bottom material and vegetation type and density and is best described by a map of Manning's roughness coefficient over the entire model domain. As is often the case, detailed information regarding bottom material is not available for the entire model domain. Standard practice is to then specify Manning's roughness relative to water depth resulting in a loose correlation with vegetation density. Eddy viscosity, or lateral mixing, also varies over the entire domain but is also dependent upon numerical element size and predicted current velocity in the model. Eddy viscosity is, therefore, specified based on a function calculated at each element for each time step. The final set of eddy viscosity and Manning's roughness values which provided the best fit between measured and simulated water elevations and flow velocities at measurement stations within the estuarial system were implemented.

NOS predicted tides and currents were used to check the model calibration at the locations shown in Figures 5-3 and 5-4. Figures 5-5 and 5-6 show results for selected calibration

locations, for water surface elevations and current velocities, respectively.

Comparisons of the NOS predicted and UCB-FEM modeled data show excellent correlation to both tidal phasing and amplitudes. Tables 5-2 and 5-3 show the statistical comparison of the model results to NOS predicted data at each station subdivided by geographical regions. Statistics are calculated for overall calibration correlation and peak condition amplitudes. Percent error is calculated by dividing the RMS (root mean square) error by the calculated mean range.

Table 5-2: Water Surface Elevation Calibration Statistics

	Time Series Statistics		
	Correlation	**Peak RMS Error (ft)**	**Peak RMS Error %**
Little Choptank River			
Taylor's Island	1.00	0.07	5.5%
Hudson Creek	0.98	0.07	4.9%
Choptank River			
Broad Neck Creek	0.98	0.06	4.3%
Choptank River Light	0.95	0.05	3.4%
Cambridge	0.96	0.08	5.1%
Choptank	0.92	0.06	3.3%
Eastern Bay			
Claiborne	0.96	0.10	9.0%
Miles River	0.99	0.10	7.8%
Chester River			
Love Point	0.98	0.10	8.7%
Cliff's Point	0.98	0.09	5.8%
Sassafras and Susquehanna River and C and D Canal			
Betterton	0.92	0.26	15.1%
Courthouse Point	0.99	0.17	7.1%
Havre de Grace	0.92	0.27	14.4%
Port Deposit	0.96	0.44	19.6%
Main Chesapeake Bay			
Sharps Island Light	0.92	0.07	5.1%
Poplar Island	0.95	0.06	5.1%
Bloody Point Light	0.94	0.07	6.4%
Matapeake	0.97	0.12	12.3%
Pooles Island	0.94	0.18	14.0%

Western Chesapeake Bay			
Cedar Point	1.00	0.08	6.6%
Cove Point	1.00	0.08	5.7%
Long Beach	0.96	0.08	7.6%
Chesapeake Beach	0.97	0.08	8.1%
West River	0.98	0.14	14.6%
Thomas Light	0.96	0.14	15.3%
Sandy Point	0.96	0.20	25.2%
Seven Foot Knoll Light	0.96	0.15	16.0%
Patapsco, Middle, and Gunpowder Rivers			
Fort Carroll	0.97	0.10	8.8%
Rocky Point	0.95	0.12	9.9%
Bowley's Bar	0.95	0.16	12.5%
Battery Point	0.95	0.14	11.3%

The model calibration results shown in Table 5-2 show better than 90% correlation for all locations. Predicted tidal elevation percent error is typically less than 10% with the exception of some specific areas of the model domain which are under 20%. Under-prediction of the Coriolis force and over-simplification of the bottom friction in the bay result in higher percent errors for tides along the western shore of the Bay including the Middle and Gunpowder Rivers. Tides in the main Chesapeake Bay near the PIERP represent the project area and are well predicted. Correlation in the main Bay near Poplar is about 95% and the peak tide is under-predicted by approximately 0.06 foot.

Table 5-3: Current Velocity Calibration Statistics

	Time Series Statistics		
	Correlation	**RMS Error (ft/s)**	**RMS Error %**
Main Cedar Point			
Cedar Point 1.1 nmi ENE	0.93	0.28	15.7%
Cedar Point 2.9 nmi ENE	0.96	0.34	19.7%
Main Cove Point			
Cove Point 1.1 nmi E	0.97	0.18	7.9%
Cove Point 2.7 nmi E	0.96	0.17	12.3%
Cove Point 3.9 nmi E	0.97	0.22	10.5%

Main James Island			
Kenwood Beach 1.5mi NE	0.94	0.16	19.1%
James Island 3.4 mi W	0.97	0.15	12.3%
James Island 2.5 mi WNW	0.87	0.16	10.5%
Main Sharps Island			
Plum Pt 2.1 mi N	0.96	0.11	9.1%
Sharps Is Lt. 3.4 mi W	0.95	0.15	12.8%
Sharps Is Lt. 2.1 W	0.92	0.11	9.1%
Main Poplar Island			
Holland Pt 2 mi E	0.95	0.15	18.4%
Poplar Is 2.2 mi WSW	0.96	0.20	10.2%
Poplar Island E of S end	0.90	0.54	19.7%
Main Thomas Point Shoal			
Thomas Pt Shoal Lt 1.8 mi SW	0.92	0.10	8.1%
Thomas Pt Shoal Lt 0.5 m SE	0.95	0.19	10.3%
Thomas Pt Shoal Lt 2 mi E	0.97	0.11	6.6%
Main Sandy Point			
Sandy Point 0.8 nmi ESE	0.97	0.43	13.8%
Sandy Point 2.3 nmi E	0.98	0.17	7.8%
Main Baltimore			
Brewerton Channel Eastern Ext, Buoy 7	0.97	0.24	18.7%
Swan Point 1.6 mi NW	0.98	0.42	17.7%
Main Pooles Island			
Gunpowder River Entrance	0.94	0.48	38.1%
Robins Point 0.7 mi ESE	0.89	0.59	17.6%
Pooles Island 1.6 nmi E	0.98	0.23	7.6%
Main Upper			
Howell Point 0.4 mi NNW	0.97	0.49	15.8%
Turkey Point 1.2 nmi W	0.88	0.33	19.4%
Patuxent River			
Hog Point 0.6 mi N	0.92	0.09	6.9%
Choptank River			
Sharps Is Lt. 2.3 mi SE	0.97	0.19	9.0%
Holland Pt 2 mi SSW	0.94	0.09	12.9%
Chlora Pt 0.5 mi SSW	0.93	0.16	11.8%
Cambridge Highway Bridge W of Swingspan	0.97	0.28	22.6%
Poplar Pt S of	1.00	0.08	3.1%

Eastern Bay			
Long Point 1 mi SE	0.88	0.21	13.5%
Tilghman Point 1 mi N of	0.92	0.12	10.9%
Parson's Island 0.7 NNE of	0.94	0.08	15.1%
Kent Island Narrows Highway Bridge	0.95	0.53	16.9%
Chester River			
Love Point 1.6 nmi E	0.95	0.29	21.0%
Hail Point 0.7 nmi E	0.96	0.17	11.0%
C & D Canal			
Arnold Point 0.4 mi W	0.87	0.21	12.95%
C & D Canal, Chesapeake City Bridge	1.00	0.01	0.13%

The above model calibration results show better than 90% correlation for most currents with the remaining better than 85%. Predicted current velocity percent error is typically less than 15% with the exception of some specific areas of the model which are closer to 20%. Near Poplar Island, the correlation is between 90% to 96%. The factors affecting tidal elevation calibration, compounded with depth averaging in the model not reflecting the variation of currents with depth in the Bay, cause the discrepancies between predicted and modeled currents.

5.3 SEDIMENTATION MODEL

Sedimentation model calibration typically requires historic sedimentation and erosion rates and detailed suspended sediment data. When these data are not available, the model can be used empirically to determine patterns and relative rates of sedimentation and erosion.

5.3.1 Non-Cohesive Sediment (Sand)

Studies performed by E2CR show fine surface sand in the vicinity of Poplar Island. The non-cohesive sediment model was run using 0.1mm (.004 inch) sediment under no-wind conditions. Analysis of results shows negligible sand transport due to tidal currents. The non-cohesive sediment model was then run for each of 16 wind directions (E, ENE, NE, NNE, N, NNW, NW, WNW, W, WSW, SW, SSW, S, SSE, SE, and ESE) for wind speeds of 4-, 13-, and 16-mph corresponding to wind speed ranges from the wind rose shown in Figure 2-4.

Modeled non-cohesive sediment transport for existing conditions is negligible for 4- and 13-mph winds for all directions. Sixteen-mph winds, when taken cumulatively with lower wind speeds, account for nearly 90% of the yearly wind occurrences and cause significant sediment transport for winds from the NNW, N and NNE directions with negligible sediment transport for winds from other directions.

Model results for 16-mph winds from the NNW, N and NNE directions are shown in Figures 5-7, 5-8 and 5-9, respectively. Other directions show negligible effects for non-cohesive sediments. Results are shown using a normalized unitless scale due to the empirical use of the sedimentation model and the lack of available data to verify model calibration.

Figure 5-7 shows areas of both erosion and accretion due to NNW winds. As shown in the figure, erosion occurs along the north, northwest and west dikes of the PIERP, about one to two thousand feet offshore of the southwest dike, at isolated patches north and east of the PIERP, and along the Eastern Shore. Areas of accretion occur along the southwest dike of the PIERP and in the deeper areas of the Poplar Island Narrows. Figure 5-8 shows increased erosion potential due to N winds, with a concomitant increase in accretion potential. As shown in the figure, erosion occurs along the north and northwest dikes of the PIERP, whereas the accretion occurs along both the west and southwest dikes. East of the PIERP, near Coaches Island and the southeast tip of the PIERP, is a relatively long stretch of erosional area, with accretion again occurring in the adjacent Poplar Island Narrows. Accretion also occurs between the southeast tip of Coaches Island and the PIERP, and south of the PIERP. Portions of the Eastern Shore also experience erosion, although less than from NNW winds. Figure 5-9 shows erosion and accretion patterns due to NNE winds. As shown in this figure, erosion and accretion from NNE winds occur only east of the PIERP. Erosion occurs in shallow, unsheltered areas east of the PIERP, Jefferson Island and Coaches Island. Accretion occurs in the deeper Poplar Island Narrows and protected areas of Poplar Harbor, between Coaches Island and the PIERP, and south of the PIERP.

5.3.2 Cohesive Sediment (Clay and Silt)

Detailed cohesive sediment data, including suspended sediment concentrations, sedimentation and erosion rates, and spatial maps of specific surface sediment properties are not available for the project area. Since these data are unavailable, the sedimentation model was used empirically

by assigning multiple thin layers of cohesive material with increasing cohesion and density over the entire domain. The layers erode and accrete in response to tidal current forcing and reach a dynamic equilibrium, meaning zero net sediment transport over a full lunar tidal cycle.

The UCB-FEM sedimentation model was initialized with nine cohesive layers of uniform thickness throughout the model domain. Layer calibration parameters include critical shear stresses of deposition (τ_{cd}) and erosion (τ_{ce}), erosion rate constant (E), bulk density (ρ), and settling velocity (w_s). The critical shear stress for deposition was set constant to 0.07 N/m^2 and settling velocity was set to 0.4 mm/second and increases as a function of concentration (Winterwerp, 1999). Other model layer parameters are shown in Table 5-4.

Sensitivity analyses show that sediment model boundary conditions are sufficiently far from the project area and have minimal impact on sediment transport in the project vicinity. Sediment model boundary conditions were set equal to the background values in the Bay. The resulting set of initial layer thicknesses shows the complete erosion of the upper layers in areas of high shear stress and deposition in quiescent areas.

Table 5-4: Sediment Model Initial Bed Layering

Layer Number	Thickness (inches)	Critical Shear Strength, τ_{ce} (N/m^2)	Erosion Rate Constant, E (g/m^2/sec)	Dry Density, ρ_{dry} (kg/m^3)
1	0.25	0.07	0.200	334
2	0.25	0.16	0.200	450
3	0.25	0.21	0.200	500
4	0.5	0.27	0.100	550
5	0.5	0.33	0.100	600
6	0.5	0.45	0.100	650
7	1.0	0.57	0.050	650
8	1.0	0.69	0.050	650
9	1.0	0.82	0.050	650

The cohesive sediment model was run for a 6-month simulation period at which point the model was operating in a dynamic equilibrium. Ensuing with-project simulations show negligible

erosion and accretion due to tidal currents. The cohesive sediment model was then run for each of 16 wind directions for wind speeds of 4- and 13-mph corresponding to wind speed ranges from the wind rose shown in Figure 2-4.

Modeled cohesive sediment transport is negligible for 4-mph. Thirteen-mph winds cause significant sediment transport for winds from the NNW, N, NNE, and NE as shown in Figures 5-10 through 5-13, respectively, with negligible sediment transport for winds from other directions. Results are shown using a normalized unitless scale due to the empirical use of the sedimentation model and the lack of available data to verify model calibration. In general, for cohesive sediments the areas of erosion and accretion are larger than for non-cohesive sediment, as properties of cohesive sediment (shape, plasticitiy, electric charge) cause the particles to remain in suspension for relatively long periods of time before they settle out.

Figure 5-10 shows erosion due to NNW winds along the northwest and west dikes of the PIERP, offshore of the southwest dikes, east of the PIERP in the shallow area near Jefferson Island and Coaches Island, and along the Eastern Shore. Accretion occurs south of the PIERP, within the sheltered portion of Poplar Harbor and in the deeper waters of Poplar Island Narrows. Figure 5-11 presents results from N winds, and shows reduced areas of erosion near the PIERP, with increased erosion along the Eastern Shore. Higher accretion potential occurs within Poplar Harbor, Poplar Island Narrows and south of the PIERP. Figure 5-12 shows model results for NNE winds. As shown in this figure, no sediment movement occurs to the west of the PIERP from NNE winds. A relatively large and strong erosion potential exists within Poplar Harbor, extending to the Poplar Island Narrows. Note that Jefferson Island creates a shadow zone where accretion occurs between it and the PIERP. Similar to all cases, accretion occurs within the Poplar Island Narrows, whereas erosion occurs north of Lowes Point along the Eastern Shore. Figure 5-13 shows model results for NE winds. This case is similar to NNE winds, although the erosion area is not as large, nor is the erosion potential as strong.

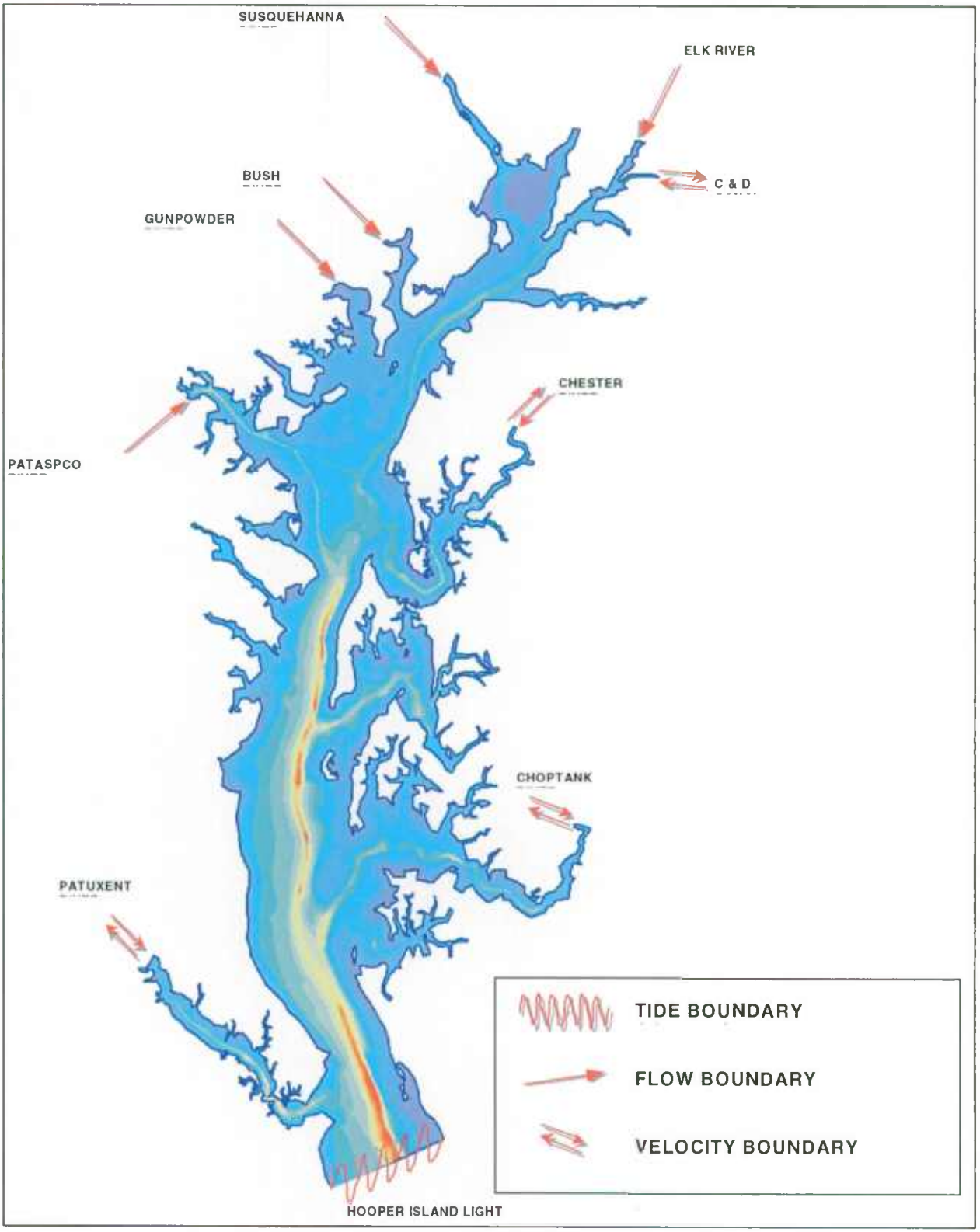

Figure 5-1: UCB-FEM Boundary Condition Locations

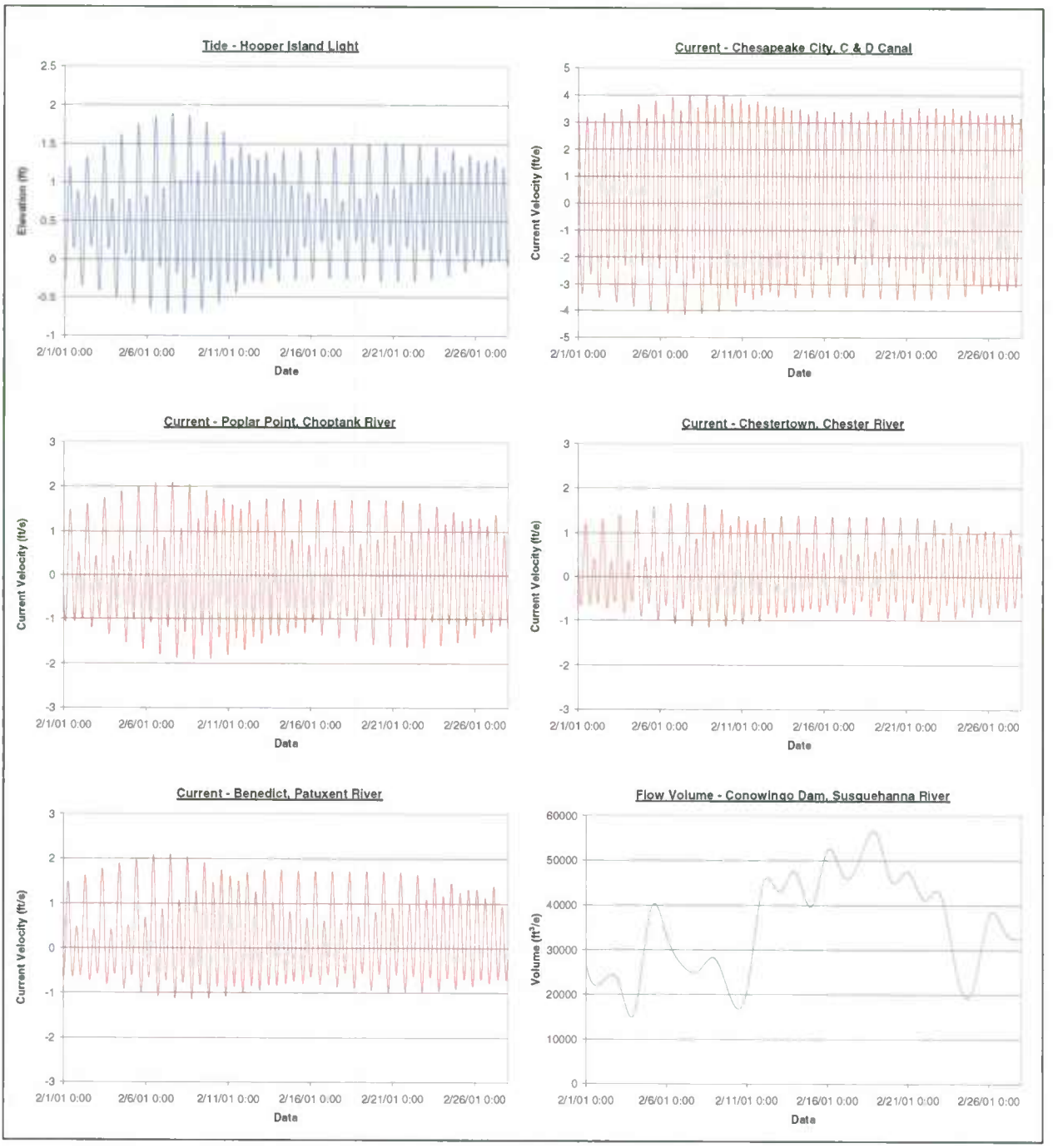

Figure 5-2: UCB-FEM Boundary Conditions

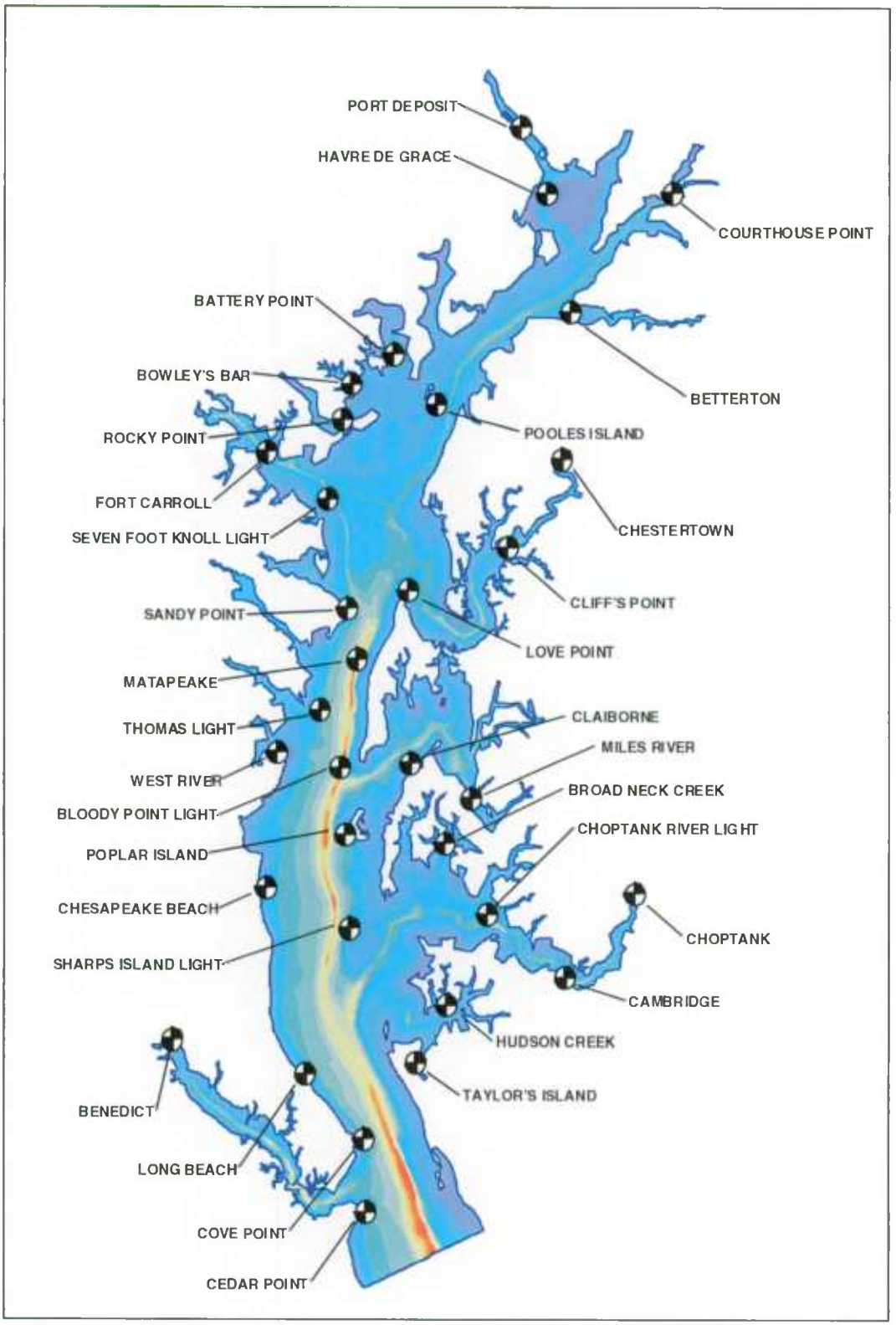

Figure 5-3: UCB-FEM Tidal Elevation Calibration Points

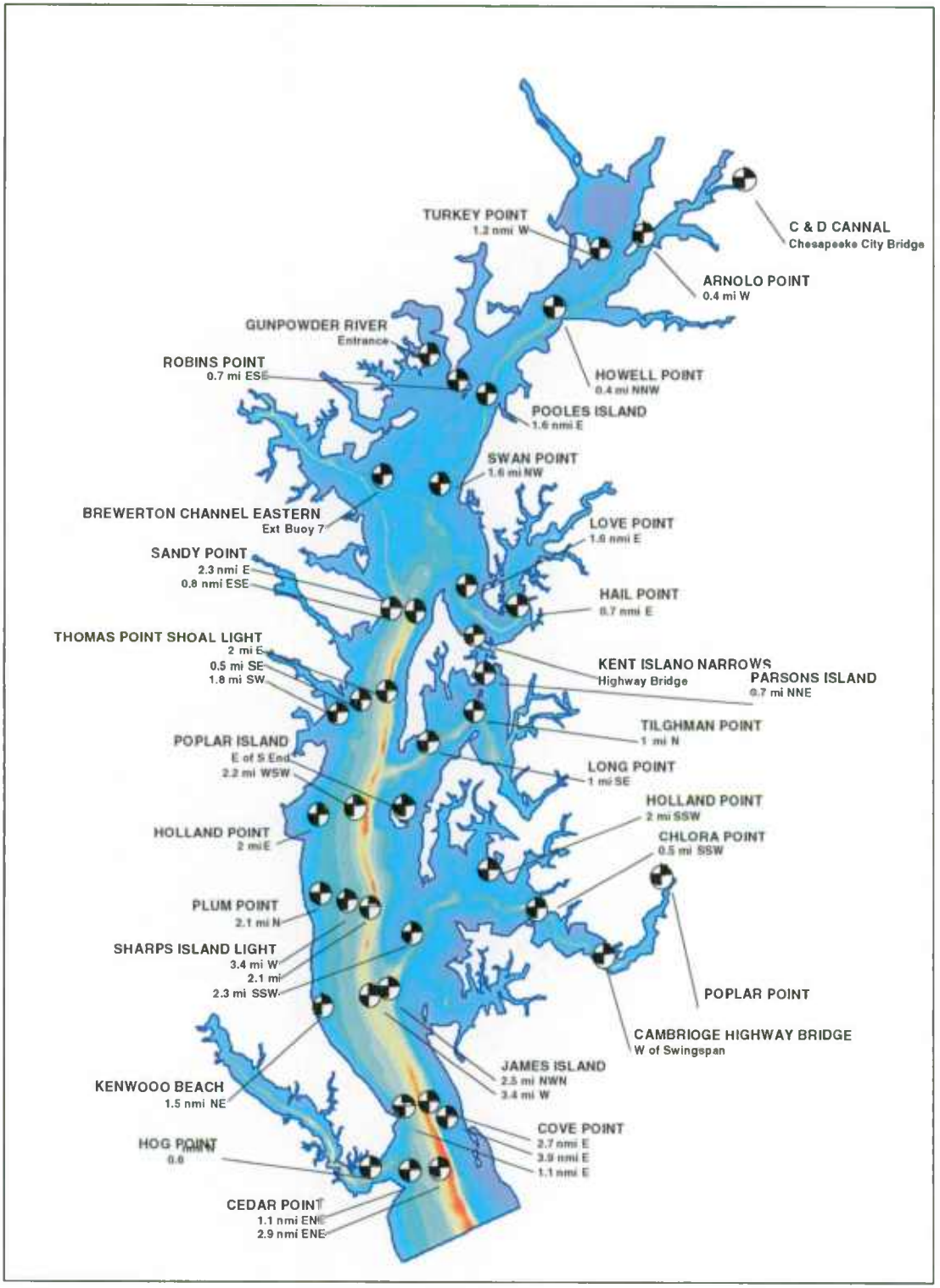

Figure 5-4: UCB-FEM Current Velocity Calibration Points

Figure 5-5: Tidal Elevation Calibration Results

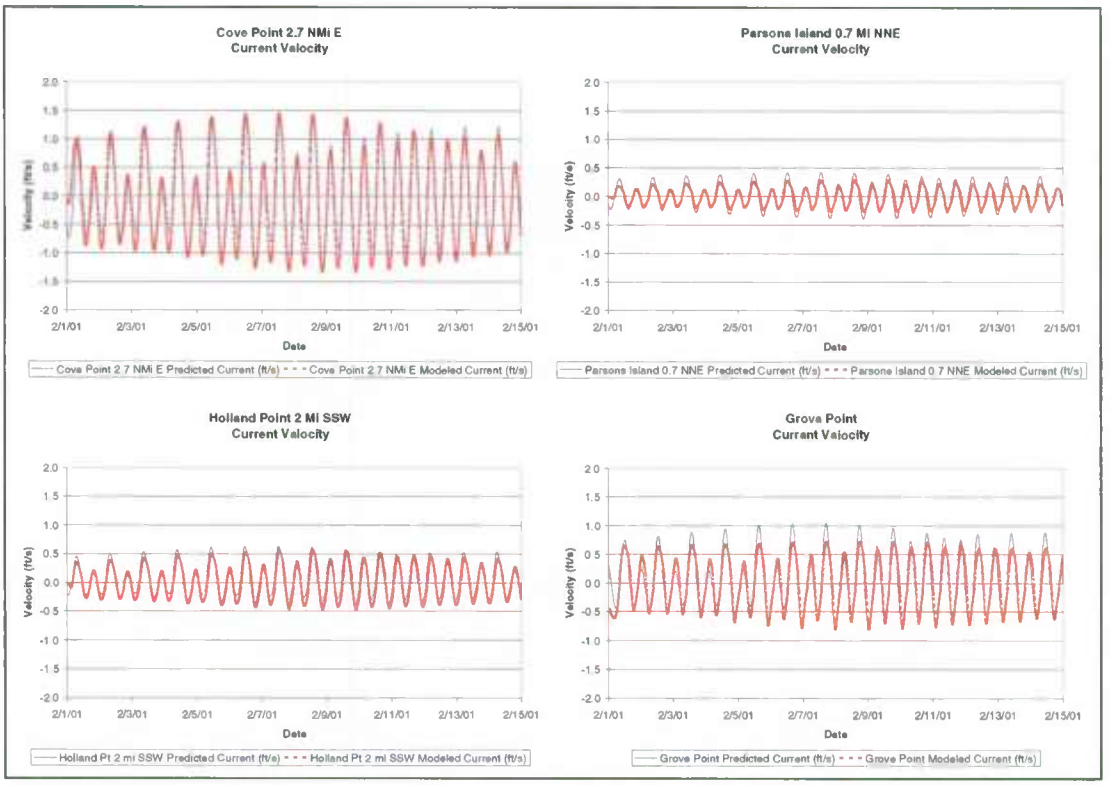

Figure 5-6: Current Velocity Calibration Results

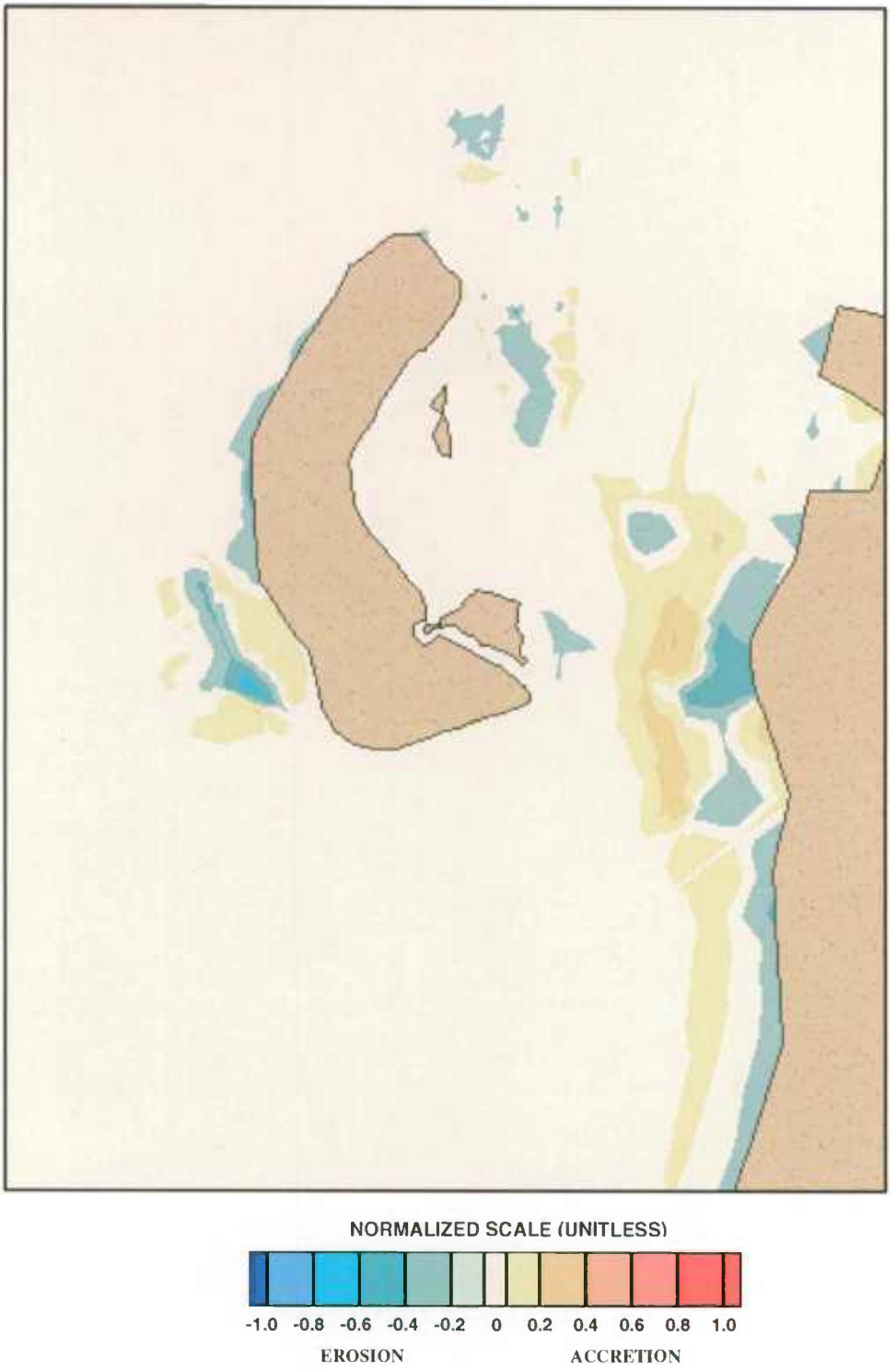

Figure 5-7: Non-Cohesive Sediment – North-Northwest Wind 16 mph - Existing Conditions

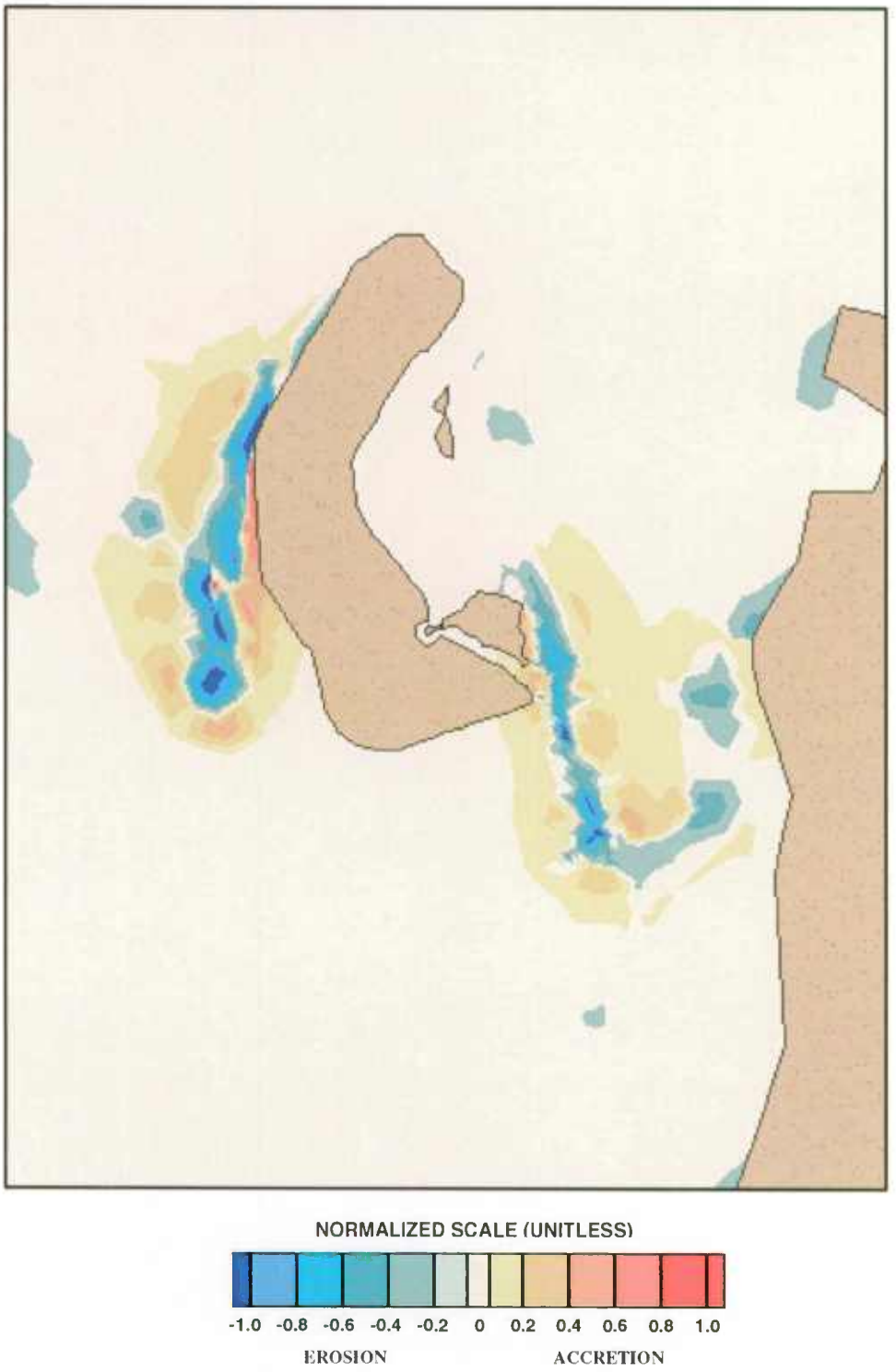

Figure 5-8: Non-Cohesive Sediment - North Wind 16 mph - Existing Conditions

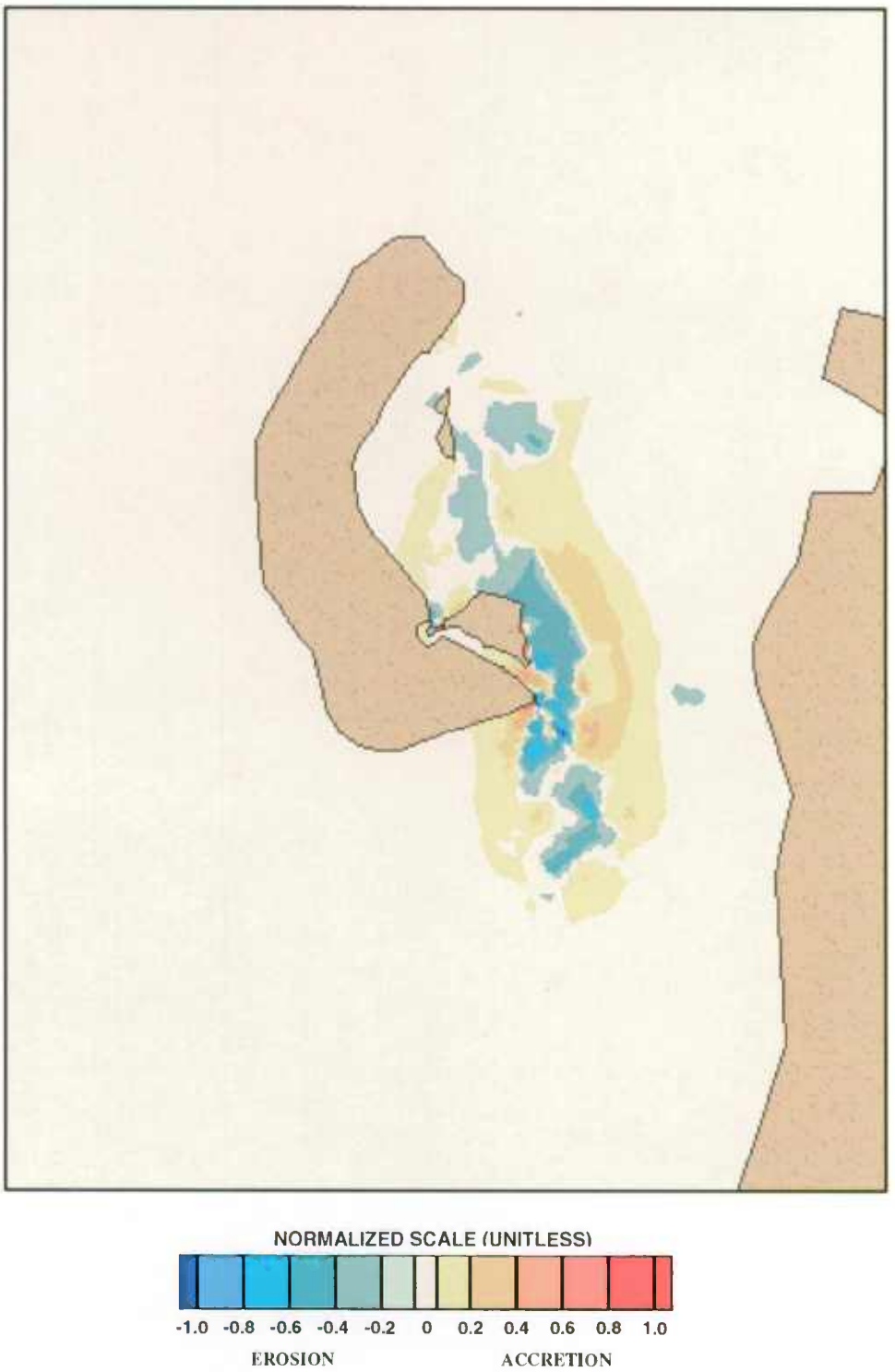

Figure 5-9: Non-Cohesive Sediment – North-Northeast Wind 16 mph - Existing Conditions

Figure 5-10: Cohesive Sediment – North-Northwest Wind 13 mph - Existing Conditions

Figure 5-11: Cohesive Sediment – North Wind 13 mph - Existing Conditions

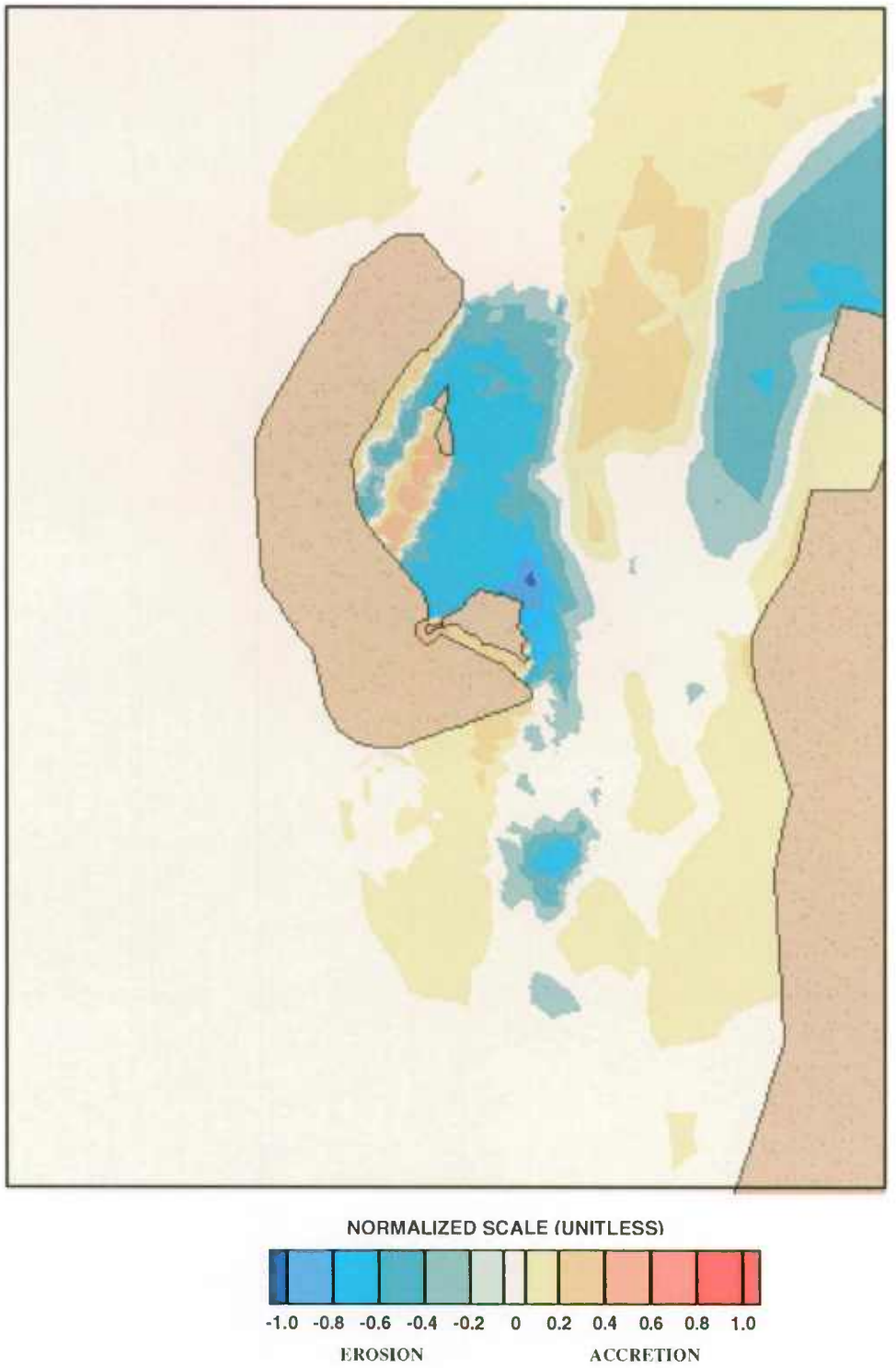

Figure 5-12: Cohesive Sediment – North-Northeast Wind 13 mph - Existing Conditions

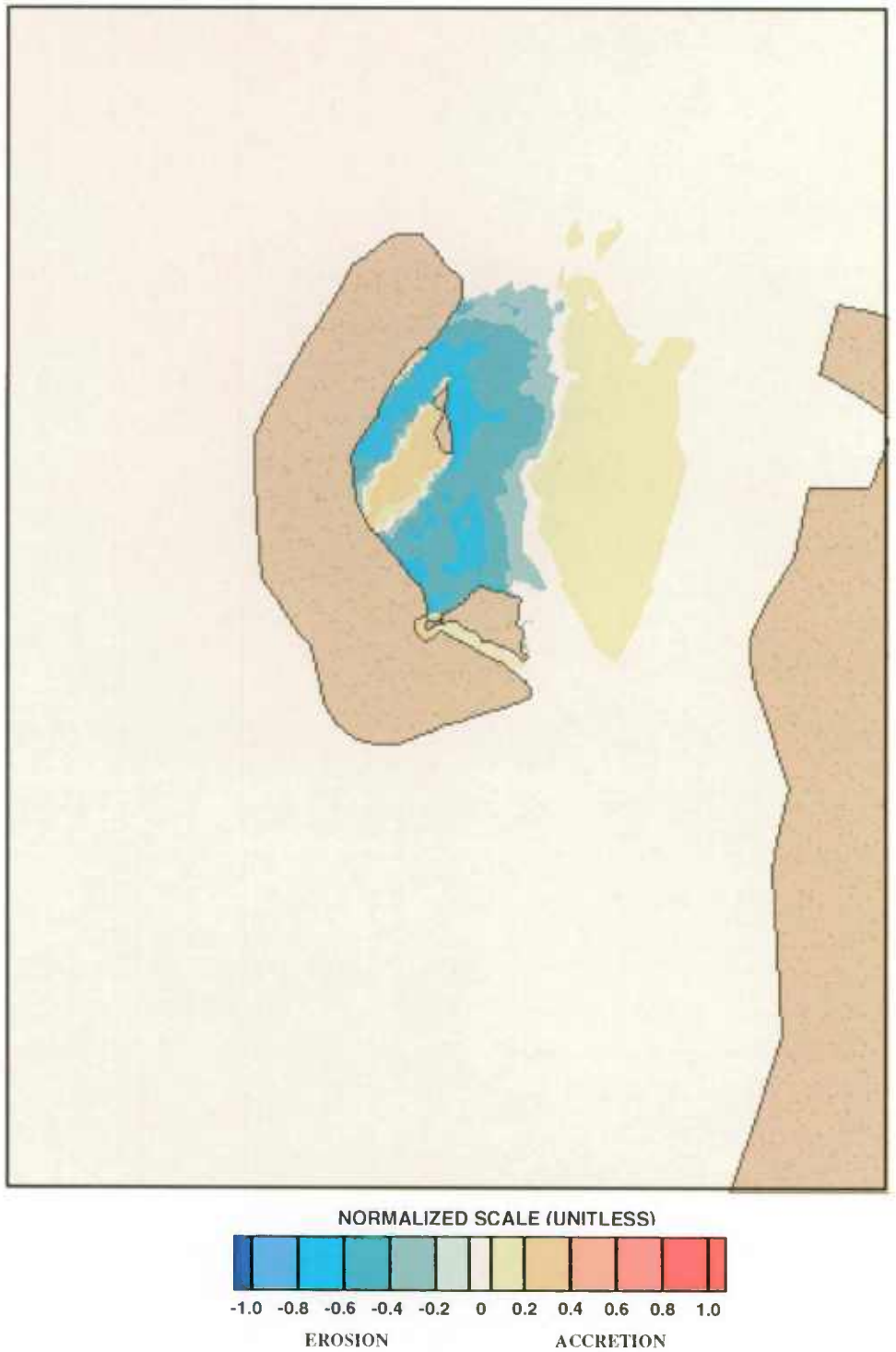

Figure 5-13: Cohesive Sediment – Northeast Wind 13 mph - Existing Conditions

6. HYDRODYNAMIC MODELING RESULTS

Evaluation of the hydrodynamic impacts of the construction of modifications to the PIERP has been conducted using the UCB-FEM model. The UCB-FEM model is used to assess impacts by applying identical hydrodynamic input boundary conditions to pre- and post- construction model bathymetry. Hydrodynamic results are then used as input into the sedimentation model which is also run using identical boundary conditions for pre- and post-construction conditions. The input conditions selected represent typical hydrodynamic conditions in the vicinity of Poplar Island.

Results of the hydrodynamic simulations are compared numerically at several points around the project site and visually for the entire project vicinity. Figure 6-1 shows the location of six comparison stations in the vicinity of Poplar Island. The following sections describe the impacts of project construction on hydrodynamics.

Hydrodynamic model results indicate that water surface elevations would be unaffected by construction of Option 6 (Figure 6-2). This is not surprising considering that the area of the modification is small compared to the Bay. Relatively small impacts, however, do occur to current velocities. Figures 6-3 and 6-4 visually show the differences in peak current velocity in the project area due to construction of the project. Peak ebb and flood currents in the Bay, generally move from north to south. The current direction changes, however, as the flow moves into and out of Eastern Bay and trains along the PIERP. At the north end of the PIERP, flow direction is practically east to west. Following construction of Option 6, flow would be displaced northward, and current velocity would increase at the northernmost point. Current velocity decreases where flow is blocked by the island, creating an area of increased quiescence to the east, west and immediately south of the Option 6 area. During the peak flood tide, shown in Figure 6-4, flows are reversed but patterns of velocity change are similar to those observed for ebb flow conditions.

Currents near the PIERP are on the order of 0.1 to 1.2 ft/sec, and construction of the additional beneficial use area does not significantly change current velocities in the surrounding vicinity. There are minor velocity increases of about 0.04 to 0.2 ft/sec north and south of the island, with decreased current velocity of about 0.04 to 0.2 ft/sec in the lee of the tidal flow to the east and

west of Option 6. South of Option 6, within Poplar Harbor, velocities are also decreased. Figure 6-5 graphically shows the differences between current velocities at six locations in the vicinity of newly created habitat area. Numerical comparisons of peak current velocity hydrodynamic modeling results for Option 6 are shown in Table 6-1.

Table 6-1: Hydrodynamic Modeling Results – Option 6

	Existing Conditions		Option 6	
	Peak Flood Current (ft/s)	*Peak Ebb Current (ft/s)*	*Peak Flood Current (ft/s)*	*Peak Ebb Current (ft/s)*
Northwest of Project	0.63	0.62	0.43	0.34
North of Project	0.43	0.44	0.61	0.70
Northeast of Project	0.38	0.31	0.08	0.11
East of Project	0.27	0.29	0.21	0.25
Southeast of Project	1.0	1.0	1.0	1.0
South of Project	0.10	0.13	0.07	0.12

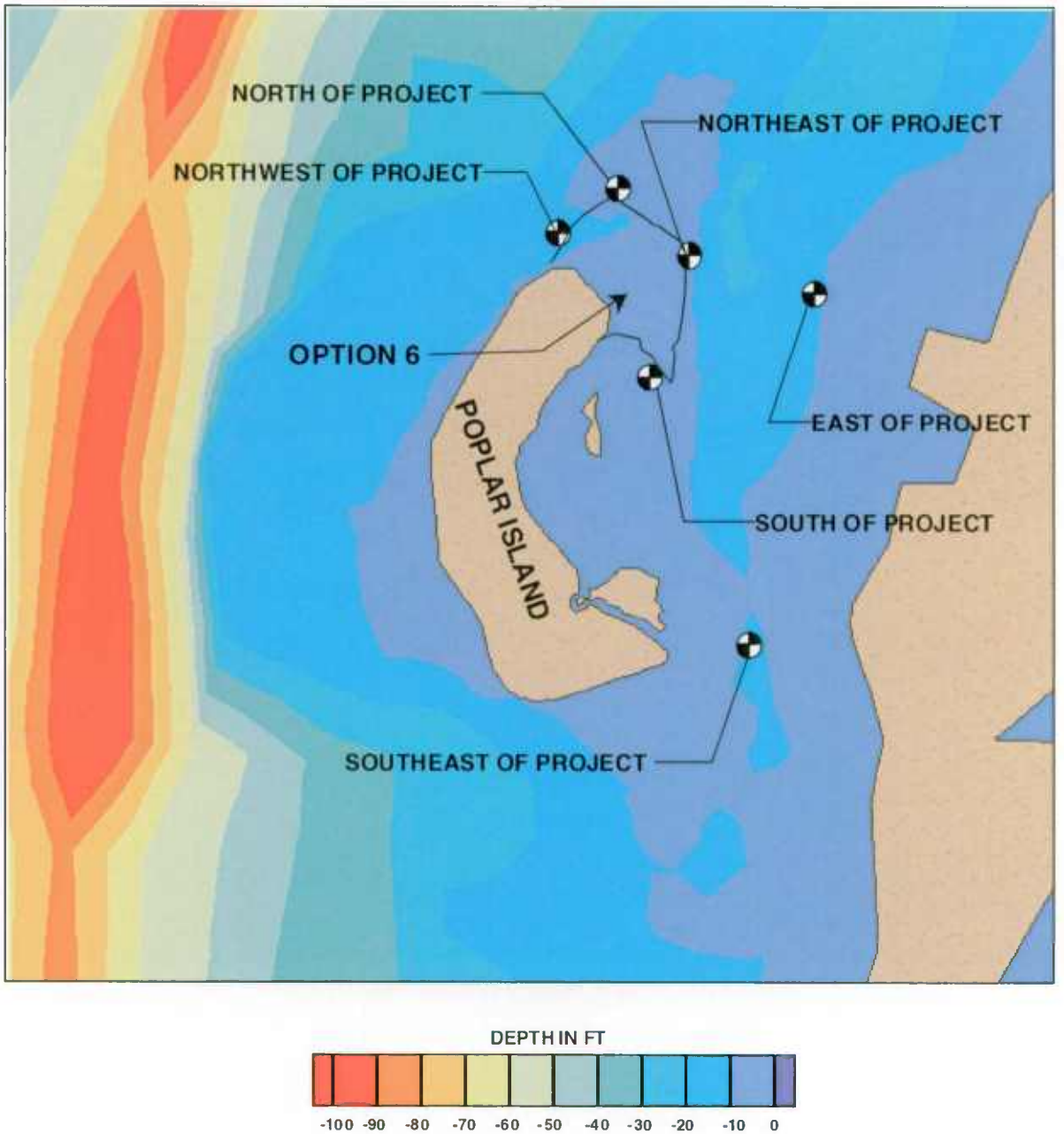

Figure 6-1: Results Comparison Locations

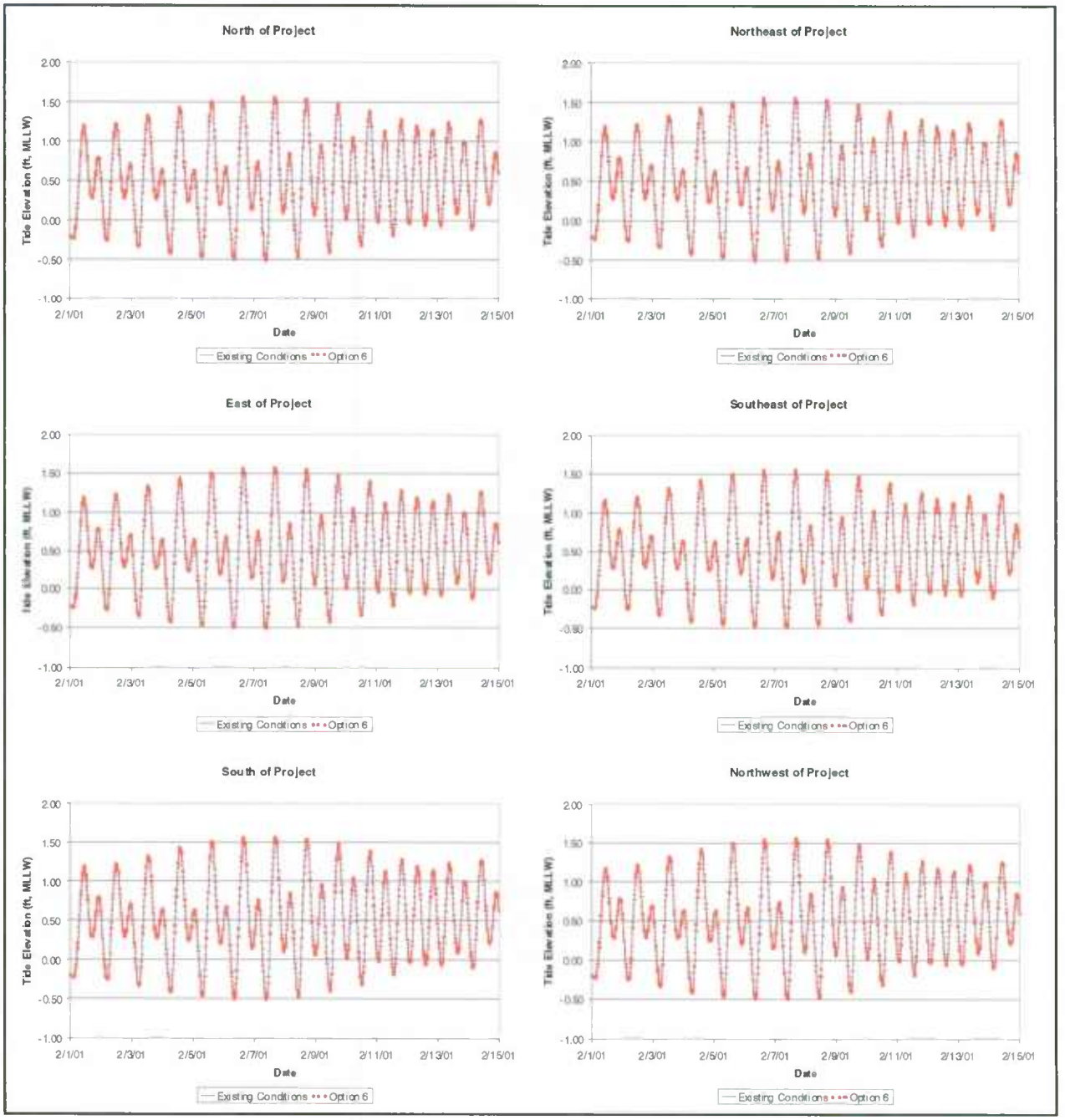

Figure 6-2: PIERP Option 6 Tidal Results Comparison

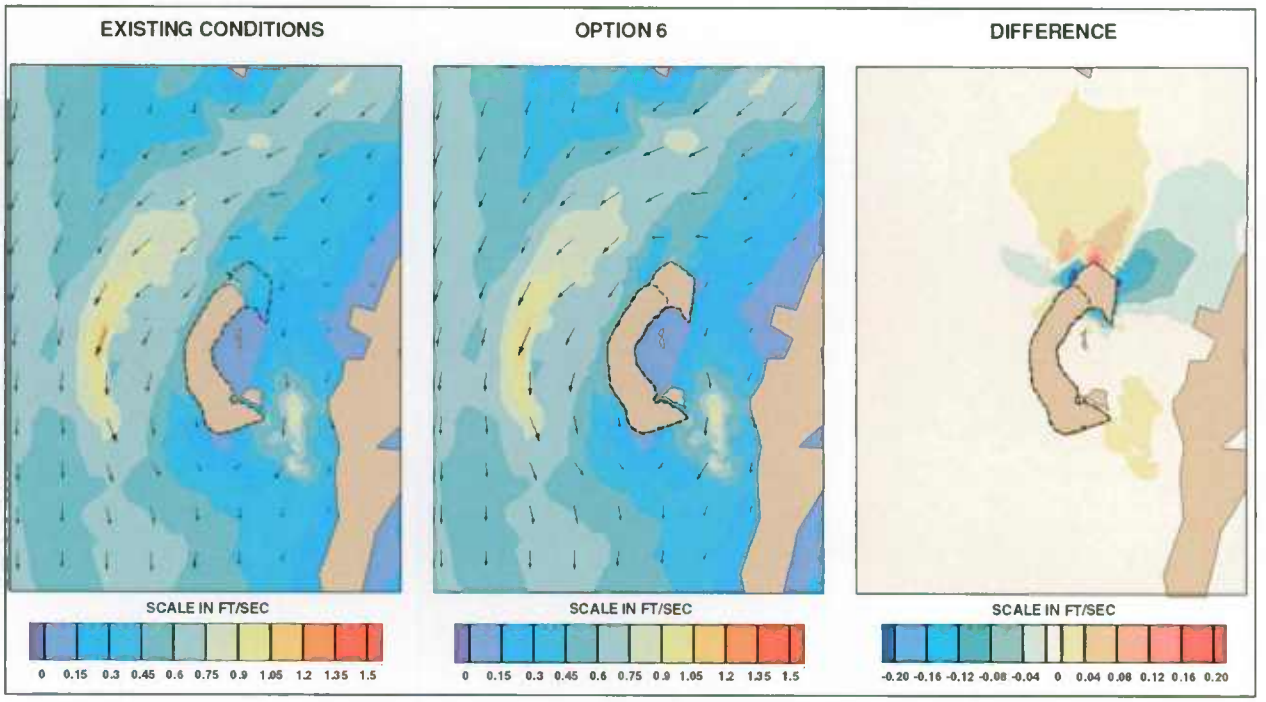

Figure 6-3: Peak Ebb Current Velocity – Option 6 vs. Existing Conditions

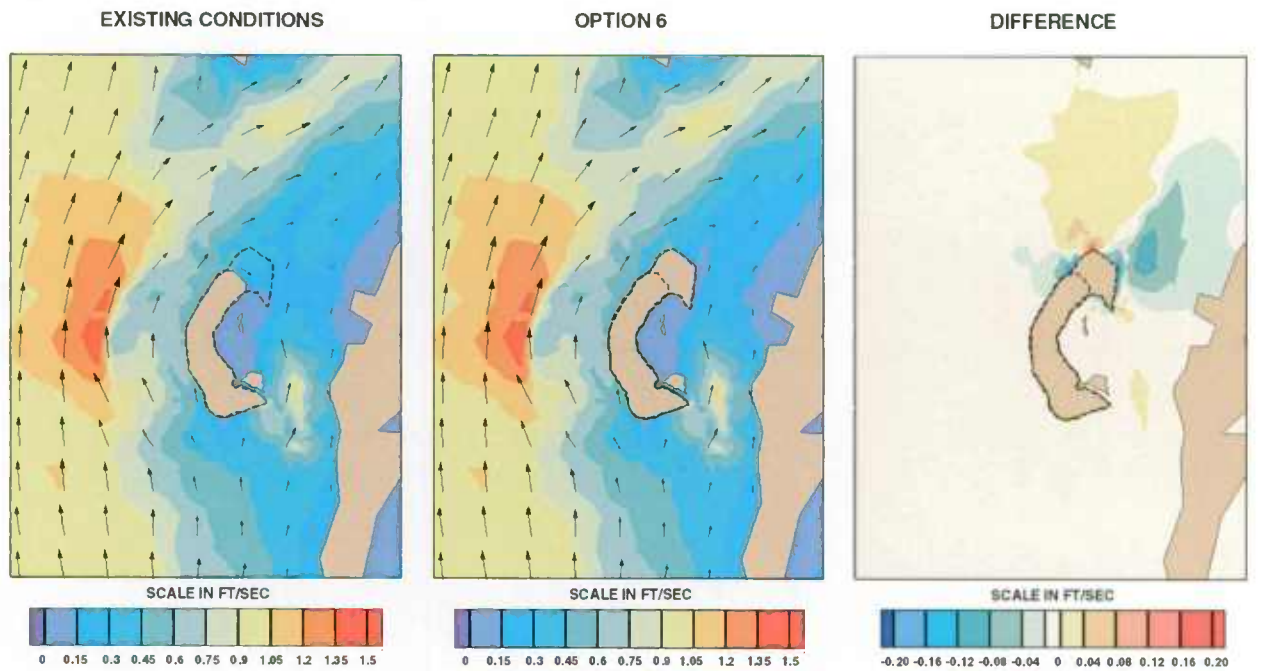

Figure 6-4: Peak Flood Current Velocity – Option 6 vs. Existing Conditions

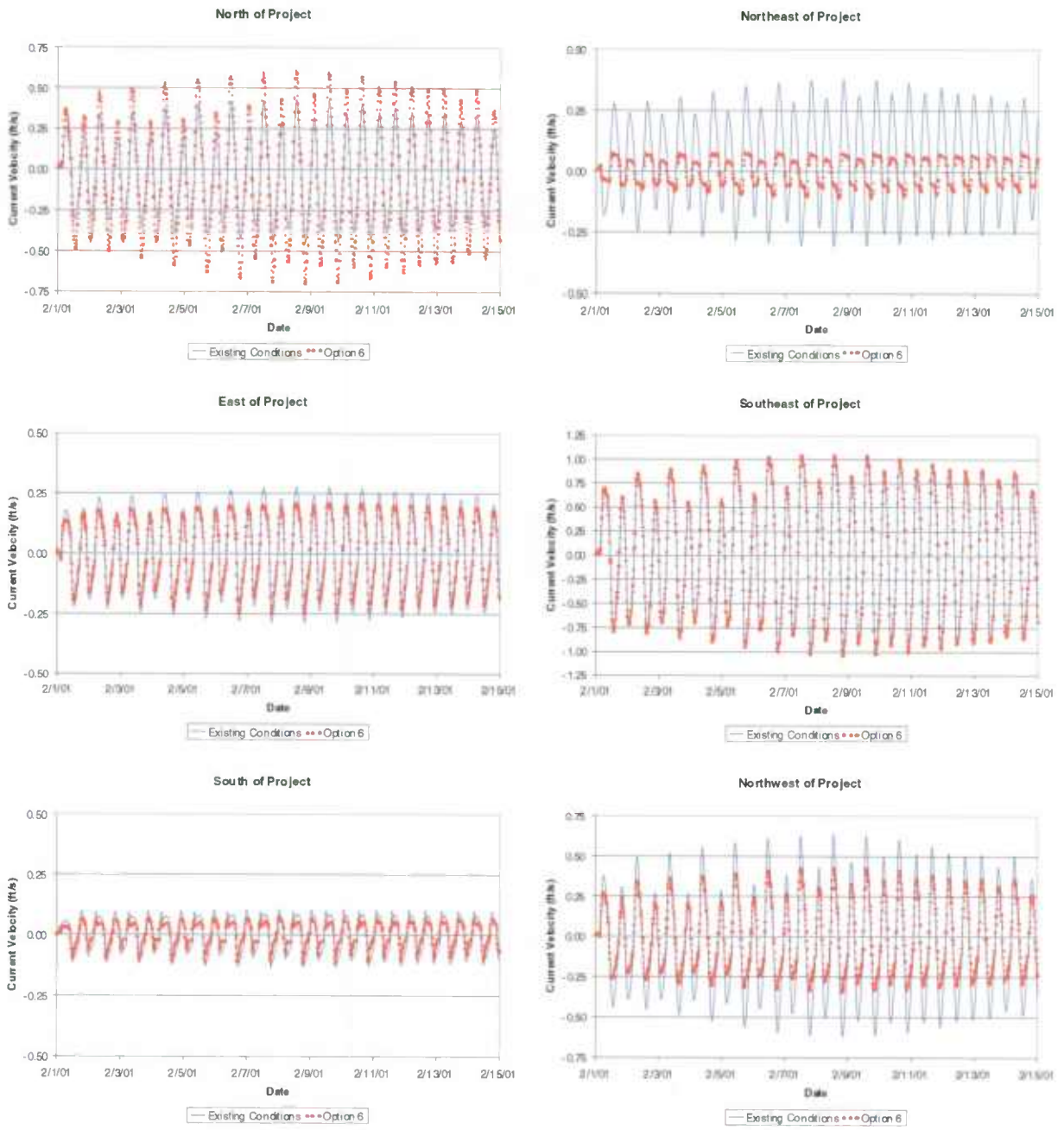

Figure 6-5: PIERP Option 6 Current Velocity Results Comparison

7. SEDIMENTATION MODELING RESULTS

7.1 GENERAL

The UCB-FEM sedimentation model was used to examine transport of non-cohesive and cohesive materials (i.e. sand and clay) which characterize sediment in the vicinity of the project site. Detailed sediment data for the vicinity of Option 6 at Poplar Island were not available so the model was used empirically by running the model to dynamic equilibrium as discussed in Section 5.3 and interpreting the results with a normalized unit scale. Examination of model results for both non-cohesive and cohesive sediments indicates that normal tidal currents in the vicinity of Poplar Island are insufficient to directly cause sediment suspension and transport. Wind generated waves increase bottom shear stresses significantly and can cause sediment suspension. Various wind speeds were modeled and 16-mph winds were determined to be the minimum necessary to cause sediment suspension and transport for non-cohesive sediments. Thirteen-mph winds were the minimum necessary to cause substantial sediment suspension and transport for cohesive sediments.

7.2 OPTION 6 MODIFICATION IMPACTS

Numerical modeling analyses indicate that sedimentation in the vicinity of Poplar Island is affected by the construction of the project. Results of the UCB-FEM sedimentation model simulations are compared visually for the entire project vicinity.

The UCB-FEM sedimentation model was run for each alignment as well as existing conditions starting each simulation with the same initial conditions. The following sections describe the impacts of each habitat construction alignment on sedimentation. Results have been normalized to a unitless scale due to the empirical use of the sedimentation model as a result of insufficient local calibration data. Cohesive sediments have properties (shape, plasticity, electric charge) that cause the particles to remain in suspension for relatively long periods of time before they settle out, resulting in a larger area affected by sedimentation and erosion than for non-cohesive sediments.

Option 6 non-cohesive and cohesive sediment model results are presented in Figures 7-1 through 7-7.

7.2.1 Non-Cohesive Sediment

Figures 7-1, 7-2 and 7-3 show sedimentation modeling results for 0.004 inch non-cohesive sediments for 16-mph NNW, N and NNE winds, respectively. Comparison of sedimentation patterns with bathymetry shows that the areas of erosion correspond to shallow water depths while deposition occurs in adjacent deep water areas.

Construction of Option 6 would interrupt the long NNW wind fetch from across the Bay, thereby reducing the rates of erosion and accretion in the lee of the project as shown in Figure 7-1. The difference plot in Figure 7-1 shows a large area southeast of the project, labeled as both "more sediment" and "less sediment" on the scale, which represents areas that are eroding and accreting under existing conditions and show no sediment transport in the with-project conditions.

Construction of Option 6 would also interrupt a large portion of the long wind fetch from the north, reducing the rates of erosion and accretion southeast of the PIERP as shown in the difference plot of Figure 7-2. The region labeled as "more sediment" and "less sediment" on the scale represents areas that are both eroding and accreting, respectively, under existing conditions, and similar to NNW wind conditions show no sediment transport in the with-project conditions.

Figure 7-3 shows that construction of Option 6 would interrupt the long wind fetch from the NNE thereby reducing the rates of erosion and accretion in Poplar Harbor. The difference plot in Figure 7-3 shows areas within Poplar Harbor labeled as "more sediment" and "less sediment" on the scale, which represent areas that are eroding and accreting, respectively, under existing conditions and show no sediment transport in the with-project conditions.

7.2.2 Cohesive Sediment

Figures 7-4 through 7-7 show sedimentation modeling results for cohesive sediments for 13-mph NNW, N, NNE and NE winds, respectively. Figure 7-4 shows a virtual absence of sediment movement within Poplar Harbor following construction of Option 6 for NNW winds, and a reduction of sediment movement east and southeast of the island. Figure 7-5 shows modeling

results for 13-mph N winds. This figure shows a potential for increased erosion and decreased accretion north of the Option 6 area after construction, due to the increased flow west of the island. The figure also shows decreased erosion of sediment from the shallow areas within Poplar Harbor and decreased deposition in the deeper areas of Poplar Island Narrows east of Option 6 and within the sheltered areas south of the PIERP. Similarly for existing conditions, 13-mph NNE winds (Figure 7-6) cause erosion of sediment within Poplar Harbor. Following construction of Option 6, a large area of Poplar Harbor, including Jefferson Island, is sheltered by the expansion, resulting in decreased erosion of sediment from the shallow areas within Poplar Harbor and decreased deposition in the deeper areas east of Poplar Harbor in the Poplar Island Narrows. Erosion of Jefferson Island is greatly reduced after construction of Option 6. Modeling results for 13-mph NE winds, Figure 7-7, show results similar to NNE winds.

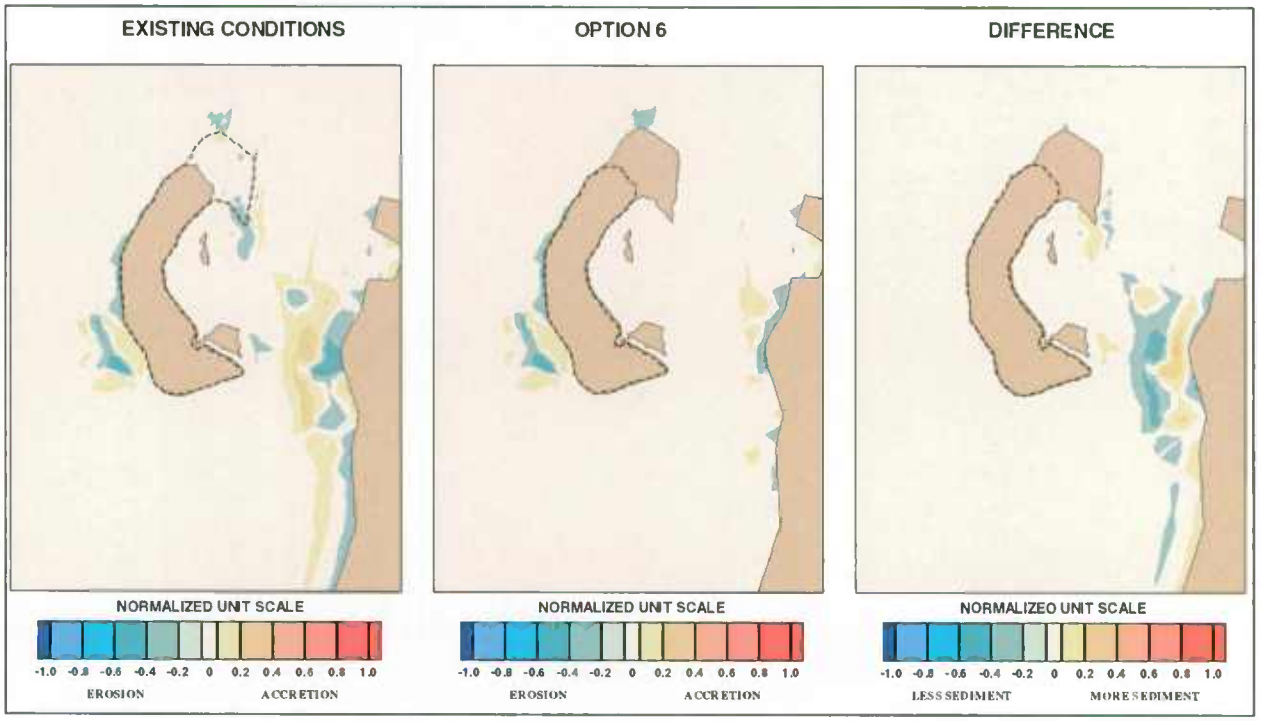

Figure 7-1: Non-Cohesive Sediment – North-Northwest Wind 16 mph – Option 6 vs. Existing Conditions

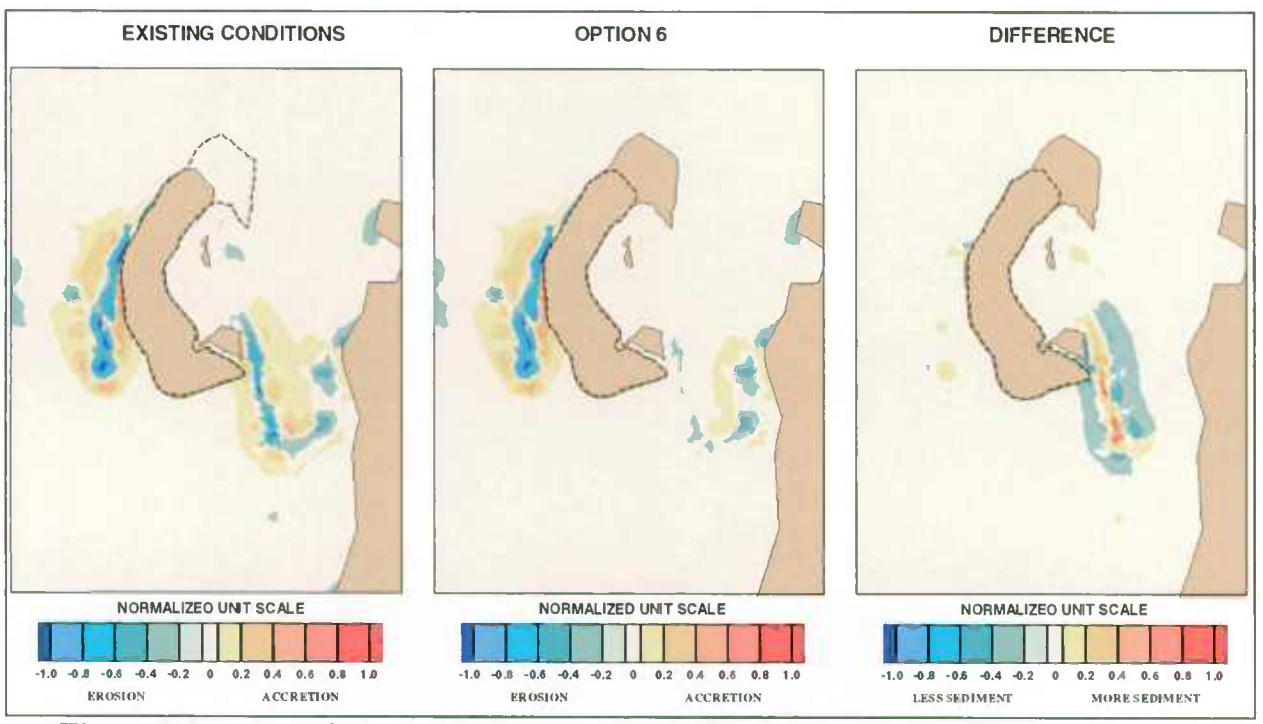

Figure 7-2: Non-Cohesive Sediment – North Wind 16 mph – Option 6 vs. Existing Conditions

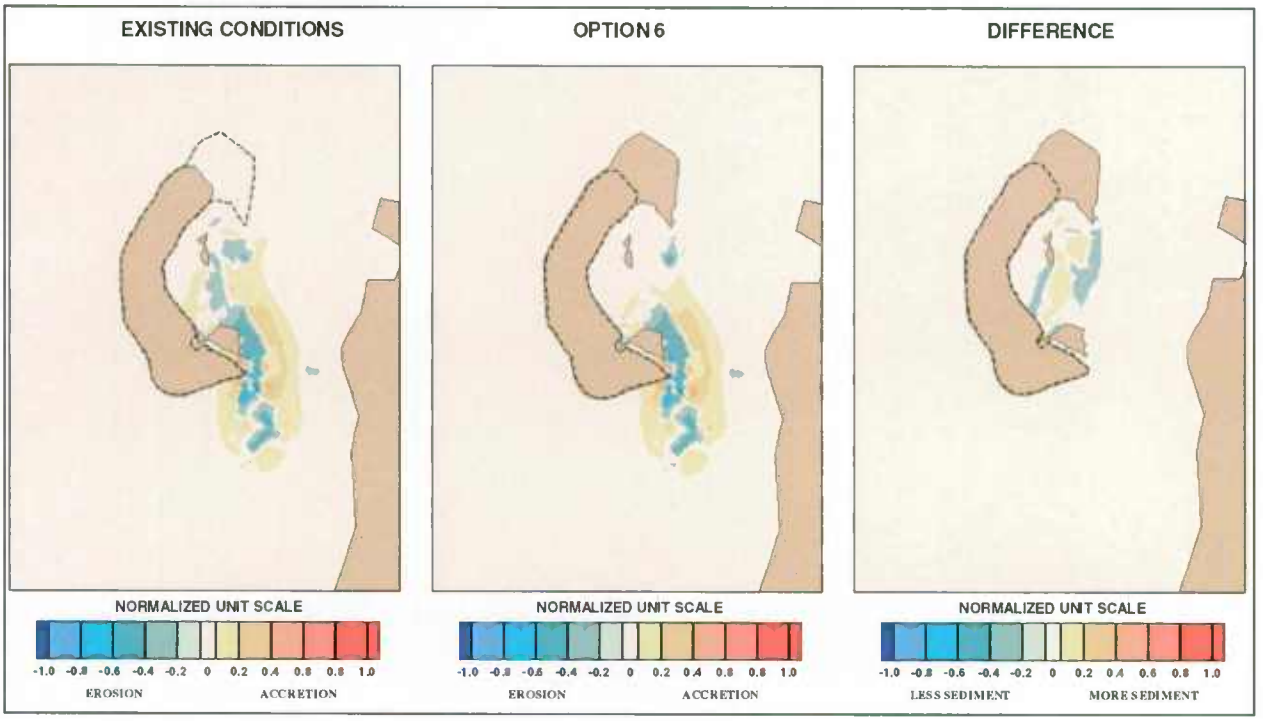

Figure 7-3: Non-Cohesive Sediment – North-Northeast Wind 16 mph – Option 6 vs. Existing Conditions

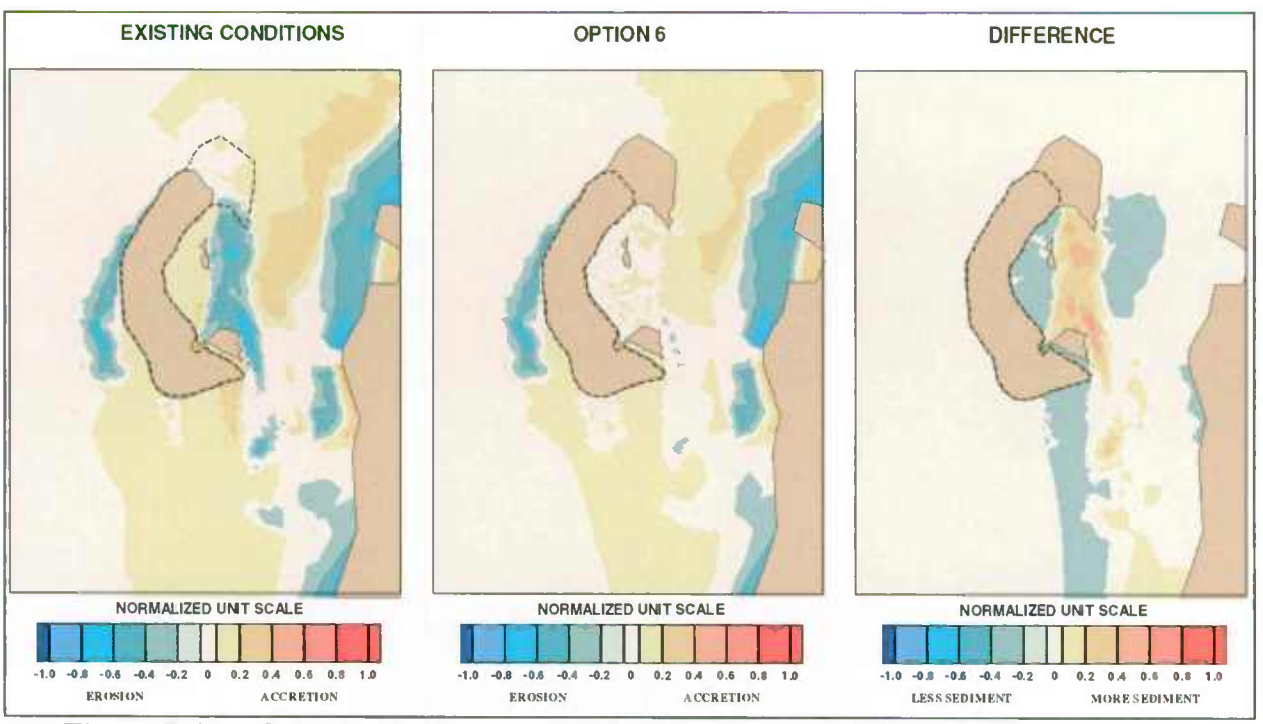

Figure 7-4: Cohesive Sediment – North-Northwest Wind 13 mph Alignment 4 vs. Existing Conditions

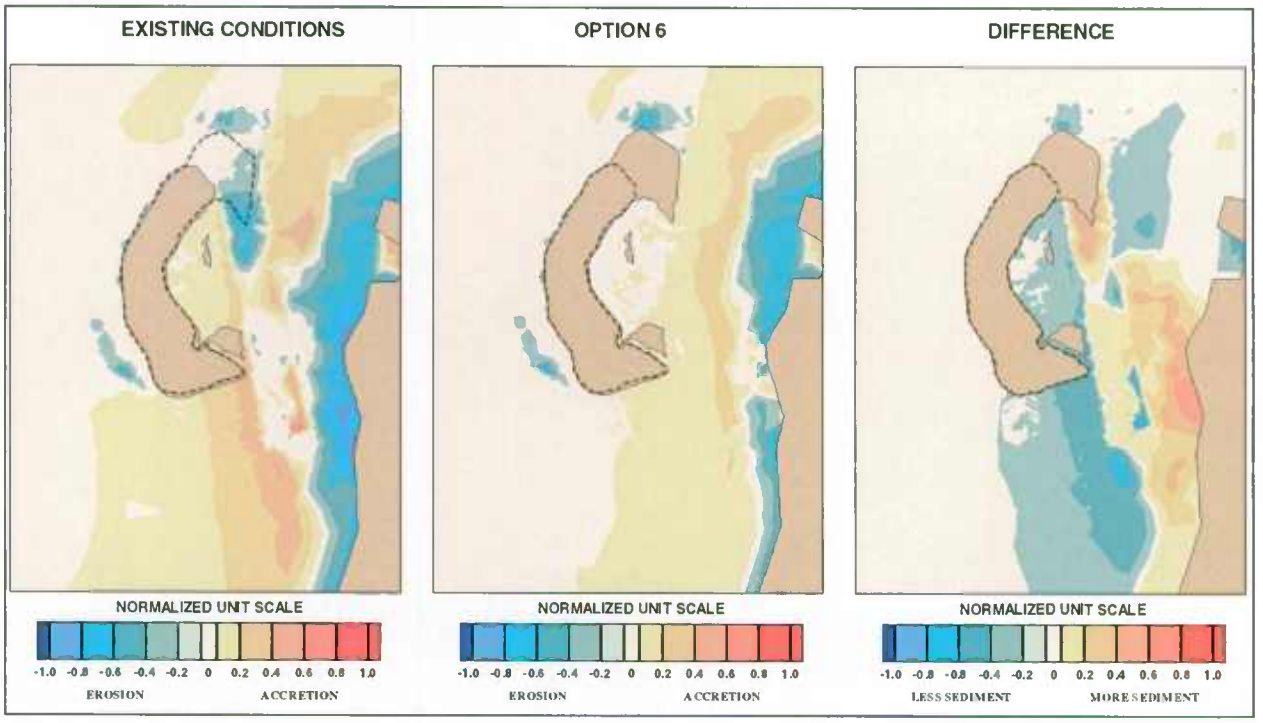

Figure 7-5: Cohesive Sediment - North Wind 13 mph – Option 6 vs. Existing Conditions

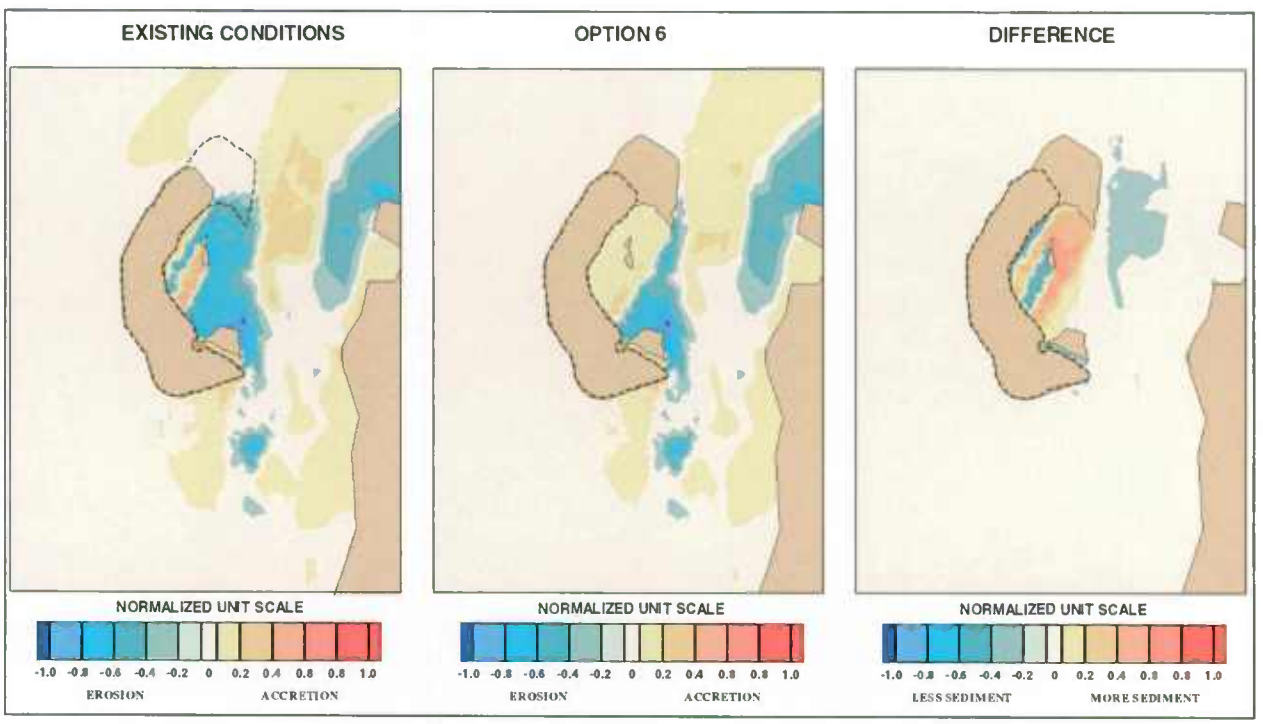

Figure 7-6: Cohesive Sediment – North-Northeast Wind 13 mph – Option 6 vs. Existing Conditions

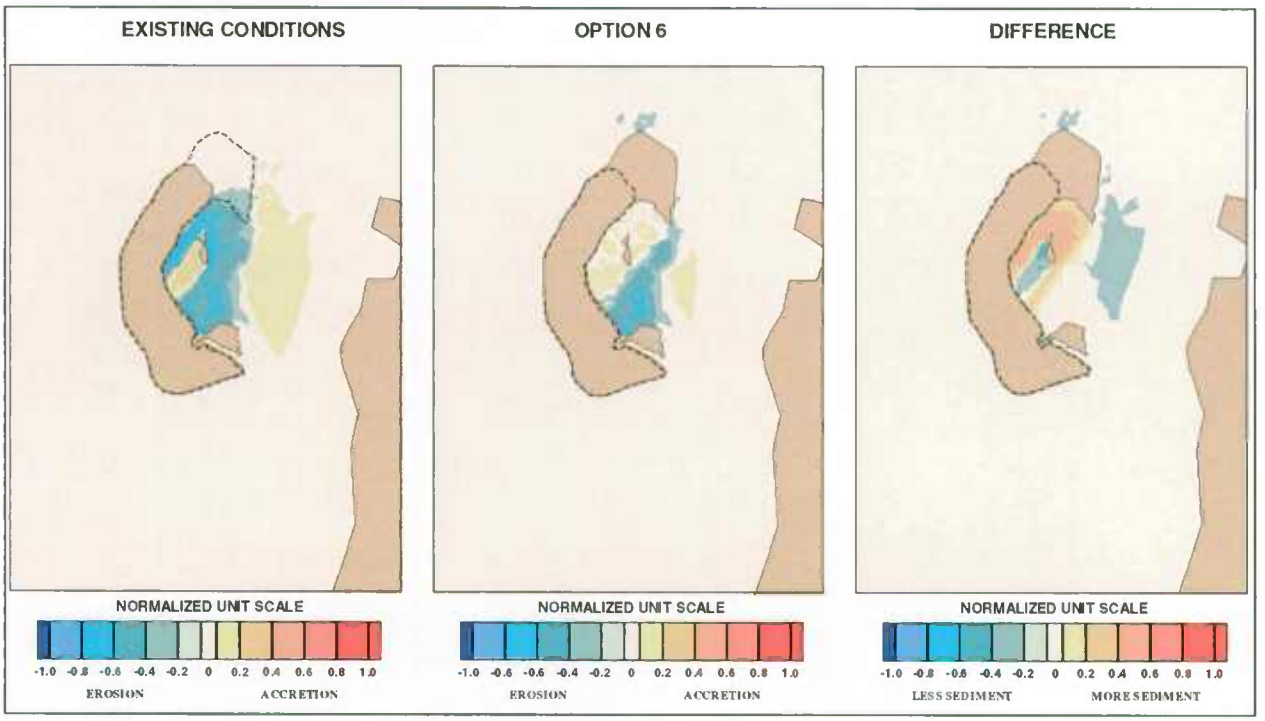

Figure 7-7: Cohesive Sediment – Northeast Wind 13 mph – Option 6 vs. Existing Conditions

8. CONCLUSIONS AND RECOMMENDATIONS

8.1 CONCLUSIONS

Results of the Hydrodynamics and Sedimentation Numerical Modeling for the Poplar Island Modifications Reconnaissance Study show that the expansion of the island to create additional beneficial use habitat area would have impacts on local conditions, especially in the area north, west and east of the island, and negligible impacts in the far field. The primary impacts on local conditions include substantial reduction of shoreline erosion along Jefferson Island and Coaches Island and improved water quality within Poplar Harbor due to creation of a quiescent area within Poplar Harbor.

Current velocities around the north and southeast of Poplar Island increase on the order of 0.2 and 0.04 ft/sec while current velocities east and west of the Option 6 area decrease by 0.2 ft/sec due to shadowing effects. Negligible changes are seen in water surface elevations.

Potential changes in tidal current velocities, coupled with wind induced wave conditions, could cause changes in sedimentation patterns and rates. Non-cohesive sands exhibit reductions in both erosion and accretion rates following island creation. Cohesive clays have decreased sedimentation and decreased sediment movement east of the PIERP.

Note that reasonable assumptions, as regards input parameters, were made to perform this sedimentation modeling study. Because environmental conditions are constantly changing, the computed sedimentation rate will likely vary as new equilibrium conditions are reached. With this in mind, the results indicate that there will be localized changes in current velocities and sedimentation rates and patterns.

8.2 RECOMMENDATIONS

The following recommendations are made to achieve stated objectives for further evaluation and monitoring of the project area.

Further numerical modeling should be performed using three-dimensional models which will

more accurately represent hydrodynamics and sedimentation in the Chesapeake Bay. A three-dimensional model could be used to simulate vertical stratification of currents and sediments due to winds and salt wedge effects.

Additional measured data is required to improve the model calibration. Data needs include bathymetric survey, current velocity measurements, water surface elevations, and suspended sediment measurements. Water surface elevations, current velocity and sediment collection devices installed simultaneously in various locations throughout the bay and project area, and left in place for a minimum period of one month would serve to verify the model calibration. Water surface elevation and current velocities would be used to refine the hydrodynamic model; thickness of sediment and suspended sediment would be used to refine the sedimentation model.

Results obtained from the refined model would be used to examine environmental impacts including water quality as well as to optimize island alignments including fixed jetties and breakwaters.

9. REFERENCES

Brigham Young University (BYU). 1995. FastTABS 3.1 Hydrodynamic Modeling Software. Engineering Computer Graphics Laboratory.

Maryland Geological Survey (MGS). 1952 through 1999. Aerial Photographs.

National Ocean Service (NOS). 1988. U.S. Department of Commerce, National Oceanic and Atmospheric Administration (NOAA). Tide and Tidal Currents in the Chesapeake Bay. Rockville, MD.

National Ocean Service (NOS). 1993. U.S. Department of Commerce, National Oceanic and Atmospheric Administration (NOAA). Chart Number 12230.

National Ocean Service (NOS). 1993. U.S. Department of Commerce, National Oceanic and Atmospheric Administration (NOAA). Chart Number 12263.

National Ocean Service (NOS). 1993. U.S. Department of Commerce, National Oceanic and Atmospheric Administration (NOAA). Chart Number 12264.

National Ocean Service (NOS). 1993. U.S. Department of Commerce, National Oceanic and Atmospheric Administration (NOAA). Chart Number 12266.

National Ocean Service (NOS). 1993. U.S. Department of Commerce, National Oceanic and Atmospheric Administration (NOAA). Chart Number 12268.

National Ocean Service (NOS). 1993. U.S. Department of Commerce, National Oceanic and Atmospheric Administration (NOAA). Chart Number 12270.

National Ocean Service (NOS). 1993. U.S. Department of Commerce, National Oceanic and Atmospheric Administration (NOAA). Chart Number 12272.

National Ocean Service (NOS). 1993. U.S. Department of Commerce, National Oceanic and Atmospheric Administration (NOAA). Chart Number 12273.

National Ocean Service (NOS). 1993. U.S. Department of Commerce, National Oceanic and Atmospheric Administration (NOAA). Chart Number 12274.

National Ocean Service (NOS). 1993. U.S. Department of Commerce, National Oceanic and Atmospheric Administration (NOAA). Chart Number 12278.

National Ocean Service (NOS). 1996. U.S. Department of Commerce, National Oceanic and Atmospheric Administration (NOAA). Tidal Currents 1996. Rockville, MD.

National Ocean Service (NOS). 1997. U.S. Department of Commerce, National Oceanic and Atmospheric Administration (NOAA). Tide Datums for Selected Stations.

National Ocean Service (NOS). 2000. U.S. Department of Commerce, National Oceanic and Atmospheric Administration (NOAA). Web Site: http://mapfinder.nos.noaa.gov/. Digital Elevation Models (DEMs).

Schubel, J.R. and D.W. Pritchard, 1987. A brief physical description of the Chesapeake Bay, in Contaminant problems and management of living Chesapeake Bay resources, edited by S. K. Majumdar, L.W. Hall, Jr., and H. M. Austin, 1-32, Pa Acad. Sci., Philadelphia, PA.

Thomas, W.A., W.H. McAnally, Jr. and S.A. Adamec, Jr. 1985. A User's Manual for the Generalized Computer Program, Sediment Transport in Unsteady, 2-Dimensional Flow, Horizontal Plane (STUDH).

U.S. Department of Agriculture (USDA), Soil Conservation Service (SCS). 1973. Soil Survey of Prince Georges County, Maryland.

U.S. Geological Survey (USGS). 2000. Web Site: http://md.water.usgs.gov/historical.html

Winterwerp, Han. On the dynamics of high-concentrated mud suspensions. Delft: Delft University of Technology, Faculty of Civil Engineering and Geosciences, 1999; 1 v. (Communications on hydraulic and geotechnical engineering; rept. no. 99-3). G642 X no.99-3